DENSITY FUNCTIONAL THEORY INVESTIGATION OF DIPOLAR ULTRACOLD ATOMS IN HARMONIC TRAPS

A THESIS SUBMITTED TO
THE GRADUATE SCHOOL OF NATURAL AND APPLIED SCIENCES
OF
MIDDLE EAST TECHNICAL UNIVERSITY

BY

OKAN KARACA ORHAN

IN PARTIAL FULFILLMENT OF THE REQUIREMENTS
FOR
THE DEGREE OF MASTER OF SCIENCE
IN
PHYSICS

JANUARY 2014

Approval of the thesis:

DENSITY FUNCTIONAL THEORY INVESTIGATION OF DIPOLAR ULTRACOLD ATOMS IN HARMONIC TRAPS

submitted by **OKAN KARACA ORHAN** in partial fulfillment of the requirements for the degree of **Master of Science in Physics Department, Middle East Technical University** by,

Prof. Dr. Canan Özgen _____
Dean, Graduate School of **Natural and Applied Sciences**

Prof. Dr. Mehmet Zeyrek _____
Head of Department, **Physics**

Assoc. Prof. Dr. Hande Toffoli _____
Supervisor, **Physics Department, METU**

Examining Committee Members:

Prof. Dr. Bilal Tanatar
Department of Physics, Bilkent University _____

Assoc. Prof. Dr. Hande Toffoli
Physics Department, METU _____

Assoc. Prof. Dr. Sadi Turgut
Physics Department, METU _____

Assoc. Prof. Dr. Mehmet Özgür Oktel
Department of Physics, Bilkent University _____

Assoc. Prof. Dr. Seçkin Kürkçüoğlu
Physics Department, METU _____

Date: _____

I hereby declare that all information in this document has been obtained and presented in accordance with academic rules and ethical conduct. I also declare that, as required by these rules and conduct, I have fully cited and referenced all material and results that are not original to this work.

Name, Last Name: OKAN KARACA ORHAN

Signature :

ABSTRACT

DENSITY FUNCTIONAL THEORY INVESTIGATION OF DIPOLAR ULTRACOLD ATOMS IN HARMONIC TRAPS

Orhan, Okan Karaca
M.S., Department of Physics
Supervisor : Assoc. Prof. Dr. Hande Toffoli

January 2014, 81 pages

Following the successful localization of dipolar ultracold atoms in harmonic traps, theoretical investigation of their density profiles have attracted very large interest in the literature. In this thesis, density functional theory will be used to investigate the density profiles of ultracold dipolar atoms (e.g. Cr) in harmonic potential traps. Parameters of the problem such as harmonic well depth, magnetic moments of the atoms will be explored in order to understand their effects on the density profile.

Keywords: ultracold fermion, magnetic dipole,density functional theory, Bose-Einstein Condensation, Fermi degeneracy,second quantization

ÖZ

HARMONİK TUZAKLARDA DİPOLAR ULTRA-SOĞUK ATOMLARIN YÜK YOĞUNLUĞU FONKSİYONELİ İLE İNCELENMESİ

Orhan, Okan Karaca
Yüksek Lisans, Fizik Bölümü
Tez Yöneticisi : Doç. Dr. Hande Toffoli

Ocak 2014 , 81 sayfa

Ultra-soğuk gazlarin harmonik tuzaklarda lokalizasyonunu takiben yoğunluk profillerinin teorik olarak belirlenmesi literatürde yoğun ilgi görmüştür. Bu tezde yük yoğunluğu fonksiyoneli kullanılarak ultra-soğuk dipolar atomların (örneğin Cr) harmonik potansiyel altında yoğunluk profilleri incelenecektir. Harmonik kuyu derinliği, atomlarin manyetik momenti gibi problem parametreleri geniş bir biçimde incelenecektir.

Anahtar Kelimeler: ultra-soğuk fermiyon, manyetik dipol, yoğunluk fonksiyoneli teorisi, Bose-Einstein yoğunlaşması, Fermi dejenerasyonu,ikinci kauntizasyon

To Omayra...

ACKNOWLEDGMENTS

I wish to express my deepest gratitude to my supervisor Assoc.Prof.Dr.Hande Toffoli for her guidance, limitless patience and understanding. She has always supported and encouraged me to keep on in my hard times.

I would like to thank to Tuğberk, who has always put up with me. He tolerated all my mental alienation and hysteria. I am lucky that I have three loving cat-mates, Pantufya, Dominique and Pancar. They give hopes and fate for living. I feel lucky to know Eda, who has always supported me and my studies by making tea and being a perfect study-mate, even though she studies on the social science.

I have to mention my legendary three evil friends to avoid future life-threatening reactions. I am grateful to Merve, Mustafa and Gökhan for their pretty evilness to everyone except me and support me to be evil without drawing reaction. I want to thank to my former classmate and current roommate Vedat Ali, who always tried to be friendly, even though this issue is harder than the millennium price problem for him.

TABLE OF CONTENTS

ABSTRACT v

ÖZ vi

ACKNOWLEDGMENTS viii

TABLE OF CONTENTS ix

LIST OF FIGURES xiii

LIST OF ABBREVIATIONS xv

CHAPTERS

1 INTRODUCTION 1

1.1 Scope of the Thesis 1

1.2 Structure of the Thesis 2

2 BACKGROUND 3

2.1 Experimental Literature 3

2.1.1 Cooling 4

2.1.1.1 Laser Cooling 4

2.1.1.2 Evaporative Cooling 5

2.1.2 Trapping 6

2.1.2.1 Magnetostatic Trapping 6

2.1.2.2 Magneto Optical Trapping (MOT) . . 6

2.1.2.3 Optical Dipole Trapping 7

2.1.2.4 Electrostatic Trapping 7

2.1.3 General Experimental Procedure 7

2.1.3.1 Fermions 8

2.2 Theoretical Literature 9

2.2.1 Bosons 9

2.2.2 Fermions 11

2.2.2.1 The Variational Principle 12

2.2.2.2 Thomas - Fermi - (Dirac) Approximation 12

2.2.2.3 The Hartree-Fock (HF) Approximation 14

2.3 Density Functional Theory 15

2.3.1 Historical Development 15

2.3.2 The Many-Body Hamiltonian and Energy Functional 17

2.3.3 The Hohenberg-Kohn Theorems 20

2.3.3.1 First Hohenberg-Kohn Theorem: Proof of Existence 20

2.3.3.2 Second Hohenberg-Kohn Theorem: Variational Principle 22

2.3.4 The Kohn-Sham Method 22

3 THE DIPOLAR FERMI GAS 25

3.1 The Model 25

3.2 Rescaling the Hamiltonian 27

3.3 The Kohn-Sham Orbitals 27

3.3.1 The Basis Functions 29

3.4 The Exchange-Correlation Energy 34

3.4.1 First Order Correction 38

3.4.2 Second Order Correction 42

4 THE NUMERICAL ALGORITHM 45

4.0.3 The Predefined Constants 45

4.0.4 The Generic Functions 45

4.0.5 The Basis Function Construction 46

4.0.6 The Hartree Potential 47

4.0.7 The Hamiltonian Matrix Construction 47

4.0.8 The Density Construction 48

4.0.9 The Energy Minimization 49

5 RESULTS AND DISCUSSION 51

5.1 Preliminary Evaluations 51

5.1.1 Choice of R_{cut} 51

5.1.2 The Number of the Basis Functions 52

5.2 The Density Profile for the Parameter g 54

5.3 The Density Profiles as a function of Number of Particles, N_P 70

6 CONCLUSION 75

REFERENCES 79

LIST OF FIGURES

FIGURES

Figure 3.1 Schematic definition of the angle θ_{ij} 26

Figure 3.2 The radial part of $\psi_{klm}(r, \theta, \varphi)$ for various (k, l) 33

Figure 3.3 $\psi_{klm}(r, \theta, \varphi)$ for various (k, l, m) 33

Figure 3.4 The direct interaction in the first order correction 39

Figure 3.5 The exchange interaction in the first order correction 40

Figure 3.6 The intersecting Fermi spheres 41

Figure 3.7 The direct interaction in the second order correction 43

Figure 3.8 The exchange interaction in the second order correction 43

Figure 5.1 The Hartree energy vs. R_{cut} for the Gaussian density distribution . 52

Figure 5.2 The exchange energy at $g = 10.0$ for the various numbers of basis functions, N_B 53

Figure 5.3 The Hartree energy at $g = 10.0$ for the various numbers of basis functions, N_B 53

Figure 5.4 The total energy at $g = 10.0$ for the various numbers of basis functions, N_B 54

Figure 5.5 The Exchange energy for $K = 4$ 55

Figure 5.6 The Hartree energy for $K = 4$ 55

Figure 5.7 The total energy for $K = 4$ 56

Figure 5.8 The density profiles of planes for $z = 0$, $y = 0$, $x = 0$ respectively for the various g 56

Figure 5.9 The contour plots of the density profiles of planes for $z = 0$, $y = 0$, $x = 0$ respectively for $g = 10$ 61

Figure 5.10 The isosurfaces of the various density values for the parameter $g = 10$ 62

Figure 5.11 The contour plots of the density profiles of planes for $z = 0$,$y = 0$,$x = 0$ respectively for $g = 7.0$ 63

Figure 5.12 The isosurfaces of the various density values for the parameter $g = 7$ 64

Figure 5.13 The contour plots of the density profiles of planes for $z = 0$,$y = 0$,$x = 0$ respectively for $g = 17.0$ 65

Figure 5.14 The isosurfaces of the various density values for the parameter $g = 17$ 66

Figure 5.15 The contour plots of the density profiles of planes for $z = 0$, $y = 0$, $x = 0$ respectively for $g = 35.0$ 67

Figure 5.16 The isosurfaces of the various density values for the parameter $g = 35$ 69

Figure 5.17 The exchange energy at $g = 10$ for the various numbers of particles, N_P 70

Figure 5.18 The Hartree energy per particle at $g = 10$ for the various numbers of particles, N_P 70

Figure 5.19 The total energy at $g = 10$ for the various numbers of particles, N_P 71

Figure 5.20 The density profiles of planes for $z = 0$,$y = 0$,$x = 0$ respectively at $g = 10$ for various N_B 71

LIST OF ABBREVIATIONS

DFT	Density Functional Theory
LDA	Local Density Approximation
TFD	Thomas-Fermi-Dirac
BEC	Bose-Einstein Condensation
BCS	Bardeen-Cooper-Schrieffer
GSL	GNU Scientific Library
KS	Kohn-Sham
HF	Hartree-Fock
Eq.	Equation
Fig.	Figure
Alg.	Algorithm
Func.	Function
MOT	Magneto Optical Trapping
TOPMT	Time Orbiting Potential Magnetic Trap

CHAPTER 1

INTRODUCTION

Ultracold atoms have been on the march after the observation of the Bose-Einstein Condensation (BEC) in 1995 [1] and the Fermi degeneracy in 2001 [12]. Even though the experimental accessibility was achieved in the last decades , the theoretical studies on the BEC and the Fermi degeneracy extends as far back as the study of Bose in 1925 [6] and Einstein [14]. Many experimental and theoretical discoveries about the BEC, the Fermi degeneracy and the ultracold atoms are achieved in the last century.

The theoretical and experimental achievements in the field of the ultracold atoms are extensively utilized many-body physics [17], [34], [42], [25], [10], [7]. Studies on the ultracold atoms promise better understanding of strongly correlated systems, superfluidity, BEC, the structural properties of the neutron stars [37], quantum phase transitions, BEC-BCS crossover and many other phenomenological studies.

1.1 Scope of the Thesis

In this thesis, the general concept of the ultracold atoms are summarized and the spatial density profile of the harmonically trapped ultracold atoms in three-dimension are investigated by using Density Functional Theory (DFT). In particular, we focus on the dilute Fermi gas with a range of magnetic moments.

The second quantization formalism with the perturbation theory is used to approximate the exchange and correlation interactions of the system. For the numerical calculations, a medium-scale code in C language is developed. The effect of the char-

acteristic parameters of the system on density profiles of the system are examined. The thesis concludes with a discussion of the results.

1.2 Structure of the Thesis

The following chapters discuss the experimental and theoretical background of the ultracold atoms, the basic concept of DFT, the theoretical examination of ultracold Fermi gas and the computational calculations in a detailed fashion. Chapter 2 reviews the historical developments of both in the experimental and theoretical sides of the ultracold atoms, the foundations of BEC and the Fermi degeneracy, while it summarizes the concept of DFT. Chapter 3 presents an investigation of the many-body Hamiltonian of the ultracold Fermi gas, deriving the exchange-correlation energy of the system by perturbation theory. Chapter 4 is a summary of the numerical algorithm with pseudo codes used in the calculation. The numerical results and analysis are given in Chapter 5. The last chapter presents the conclusions of this thesis.

CHAPTER 2

BACKGROUND

2.1 Experimental Literature

Experimental studies on ultracold atoms has become a promising field for investigation of many aspects in many-body systems thanks to developments in cooling methods and vacuum techniques. There are two milestones in experimental techniques used in the field of ultracold atoms. These are laser cooling [2], [22] and evaporative cooling [23], which gave opportunities to access to the ultracold regime, where the quantum mechanical affects become observable. Improvements in vacuum systems by novel materials and architectures provide the required isolation for ultracold atoms from surroundings, and allows obtaining high degree optical access to ultracold atom systems. Eventually, two crucial stages arise in the experiments:

- Cooling particles into range of mK-μK

- Trapping the cooled atoms in a tiny volume to achieve desired density

Even though these stages are expressed separately, they overlap in some aspects due to the experimental design used. Hence, many different experimental designs have been developed to obtain ultracold atoms. In this section, we introduce a general outline of the experimental literature.

2.1.1 Cooling

The first aspect of ultracold experiments is obviously to cool atoms to the low energy regime. Generally, laser cooling and trapping is used before evaporative cooling to obtain the desired temperature. Laser cooling and trapping ensures that the number of particles in experiments remains fixed. Evaporative cooling is used subsequently to laser cooling.

2.1.1.1 Laser Cooling

In simple terms, the logic behind laser cooling is to use momentum exchange between atoms and photons via absorption and radiation processes. In the absorption process, the frequency of the photon absorbed by the atom depends upon their relative velocities due to the Doppler effect. That makes the process velocity dependent, which is desirable to cool atoms with varying kinetic energies.

To initiate the cooling process, atom and laser beams are sent in opposite direction in vacuum environment [32]. When collision occurs, the photon is absorbed by the atom, and subsequent photons are emitted back by the atom immediately. The atom gains some of its momentum back in each emission. However, the emitted photons will be in random direction and their average momentum turns out to be zero statistically.

When the momenta of atom and photon before the collision are expressed as

$$\begin{aligned} \vec{p_a^i} &= m\vec{v}_0 \\ \vec{p_p^i} &= h\vec{k}_0, \end{aligned} \tag{2.1}$$

the momentum of the atom just after absorption becomes

$$\vec{p}_a^{ab} = m\vec{v}_0 - h\vec{k}_0. \tag{2.2}$$

Finally, once the atom re-emits photons, the momentum is

$$\vec{p}_a^{ab} = m\vec{v}_0 - h\vec{k}_0 + \langle h\vec{k} \rangle \tag{2.3}$$

where $\langle h\vec{k} \rangle$ is the total momentum of the emitted photons averaged over angles.

This last term in Eq. (2.2) becomes zero statistically. After a sufficient collision-absorption-emission processes, atoms slow down to a limit velocity, where number of they can be trapped.

There arises a problem immediately. Once atoms slow down to a limit, where Doppler shift changes and absorption frequency of the slow atoms become out of phase with the frequency of the laser beams. As a result, the slowing process ceases to work. There are two possible solutions to this problem to continue cooling. The frequency of the laser beam can be accordingly varied, which is quite expensive and the construction such a wide range laser is another challenging work. The other solution is changing the absorption frequency of atoms by using an external magnetic field. Applying a magnetic field will change the absorption frequency of atoms due to the Zeeman effect. By adjusting the magnetic field, atoms can be cooled with a narrow range laser.

The procedure explained above is the essence of laser cooling. Laser cooling by using a single source reduces control on atom collection. Hence, multiple laser sources with same frequency are usually used with different geometries in experimental setups.

2.1.1.2 Evaporative Cooling

BEC or Fermi degeneracy are observed under two principle physical conditions. Collection of atoms should be ultracold and dense enough. Laser cooling method is a notable method due to its ability to cool atoms without loss of particles in a tiny volume. Even though, the sample can be cooled to μK range via laser cooling, other problems arise due to high density of sample.

The fundamental idea behind evaporative cooling is selective removal of highly energetic atoms in the sample by lowering the trap depth [11]. When the most energetic atoms are removed from the trap, temperature of the sample decreases. The remaining atoms continue s wave collisions, and some atoms in the sample become more energetic after this collisions, while some others slow down. The sample can be cooled by continuously lowering trap depth. Beside cooling the sample, the volume of sample can also be shrunk simultaneously due to loss of atoms via decreasing the scatter-

ing length, while cooling sample. These lead to enough dense and cooled atoms as desired.

Evaporative cooling is employed following laser cooling in experiments, instead of applying it from the start, since number of atoms is not conserved in evaporative cooling.

2.1.2 Trapping

2.1.2.1 Magnetostatic Trapping

The second important task in ultracold atoms experiment is trapping cooled atoms in a confined geometry. The magnetic field can be used by itself to produce the trapping potential. The trapping process is not a distinct part of the experimental procedure. The atoms are trapped simultaneously with the cooling process. Applying a magnetic field leads to the splitting in atomic states known as the Zeeman effect. When a local minimum of magnetic field is created inside the vacuum using a distinct magnetic source in suitable geometry, the low energy configuration in the Zeeman splitting can be trapped in this local minimum pool, while the more energetic one is removed with evaporative cooling.

In a magnetostatic trap, a center with the zero field strength is not desirable, because atoms may undergo spin flip and lose the ground state. There are various solutions proposed. Non-zero center can be obtained by designing appropriate geometry of magnetic sources. However, it reduces the depth of trap. Another solution is to change the zero field center by rotating the magnetic field as in *Time Orbiting Potential Magnetic Trap (TOPMT)*. Further solution is that repelling atoms from zero field center by using laser beams [3].

2.1.2.2 Magneto Optical Trapping (MOT)

In magnetostatic trapping, only atoms with low energy configuration in Zeeman splitting can be trapped. Adding an optical component to magnetostatic trapping solves this restriction.

Basically, two laser beams with identical frequencies are directed toward the minimum magnetic field center in opposite directions along splitting axis. Atoms on both sides feel an average force toward the minimum magnetic field center due to radiation pressure caused by laser beams. Hence, clouds of atoms are forced to move toward minimum magnetic field region created with weak magnetic field described as in magnetostatic trapping method. [36]

2.1.2.3 Optical Dipole Trapping

Optical dipole trapping is based on the interaction of electric dipoles of the trapped species with the electric field component of light. Electric dipoles in an electric field experience a force proportional to the gradient of the electric field and magnitude of dipoles. Hence, an optical confinement can be crated for trapping atoms with certain electric dipoles by choosing an appropriate geometry and frequency of laser, which is not resonant with transition frequencies of any kind. [20]

2.1.2.4 Electrostatic Trapping

The principle behind this method is quite similar to magnetostatic trapping, using Stark effect instead of Zeeman effect. The Stark effect is used to trap low-energy configuration of particle in minimum region of constructed electric field geometry. Usually, this method used to trap molecules, where other methods become problematic due to complex electronic structure. [4]

2.1.3 General Experimental Procedure

The trapped species described in the previous section can be either bosonic or fermionic in nature. This section briefly discusses differences in experimental setups for different species.

2.1.3.1 Fermions

Ultracold experiment with fermions are more complicated than the bosonic case due to the fact that Pauli exclusion principle prohibits s-wave scattering, which is the basis of evaporative cooling. Unlike the bosonic case, this crucial state in cooling process cannot be applied directly to fermions. However, the remaining steps for cooling fermionic atoms are identical to the bosonic case.

In bosonic case, atoms occupy the lowest hyperfine state and undergo s-wave scattering in the evaporative cooling stage. Since, this is impossible in fermionic case, fermionic atoms are prepared in the two lowest hyperfine states by using double MOT. For instance, two lowest hyperfine states, $F = 9/2$, $m_F = 9/2$ and $m_F = 7/2$ are obtained with a 1:1 ratio in an experiment with ^{40}K and the temperature is decreased to about 300 nK, a value below the Fermi temperature [12]. It is crucial to maintain the ratio fixed to be able to continue binary s wave collision in evaporative cooling. Therefore, removing the most energetic atoms from sample has to be done in pairs from distinct hyperfine state. However, the efficiency of evaporative cooling with two distinct hyperfine state decreases drastically with increasing density as reported experimentally.

A further method to get round this restriction in the fermionic case is to cool boson-fermion mixture together. In an experimental reported by Truscott *et al.* (2001), the mixture of ^{6}Li and ^{7}Li, which are fermionic and bosonic respectively, are cooled together. Initially, two species are cooled with laser cooling separately. About 10^9 ^{7}Li and 10^6 ^{6}Li atoms at 300 μK are loaded to double a MOT.^{7}Li atoms are made to occupy the lowest hyperfine state, $F = 2$,$m_F = 2$ by a weak magnetic field and optical pump and ^{6}Li atoms made formed a mixture of the sub-states of $F = 3/2$. Next, ^{7}Li atoms are cooled by evaporative cooling. ^{6}Li atoms are cooled spontaneously due to s-wave collisions with ^{7}Li. The evaporative cycle is applied and the most energetic ^{7}Li atoms are removed from trap after each cycle. By this process, ^{6}Li can be cooled to about 240 nK [41].

2.2 Theoretical Literature

Foundation of the theory of ultracold atoms go back to the studies of Bose (1924) in photon statistics [6]. Einstein (1924-1925) extended this study to massive particles [14]. Owing to its two pioneers, the peculiar behavior of bosons below a critical temperature is known as the Bose-Einstein Condensation(BEC). BEC predicts occurrence of a phase transition, which corresponds to the lowest state condensation, in a non-interacting bosonic gas. Fritz London claimed that helium superfluidity is a consequence of BEC in 1938 [30] and this claim was verified by neutron scattering of single particle atomic momentum in 1995 [19].

2.2.1 Bosons

Bogoliubov theoretically predicted BEC in weakly interacting non-ideal gases in 1947 [5]. A more complete description of BEC wavefunction in dilute gases was given by Gross and Pitaevskii (1961).

Many-body equation governing the interacting bosons in the second quantization

$$i\hbar\frac{\partial}{\partial t}\hat{\Psi}(\vec{r},t) = \Bigg[-\frac{\hbar^2}{2m}\bigtriangledown^2 + V_{ext}(\vec{r}) + \int d\vec{r}'\hat{\Psi}^\dagger(\vec{r}',t)V(\vec{r},\vec{r}')\hat{\Psi}(\vec{r}',t)\Bigg]\hat{\Psi}(\vec{r},t) \tag{2.4}$$

where $\hat{\Psi}^\dagger$ and $\hat{\Psi}$ are the boson creation and annihilation field operators respectively.

Gross and Pitaevskii suggested that these operators can be replaced by the expectation value of these operators in lowest state, since under the condensation temperature, $T \ll T_c$, bosons interact only via s-wave interaction, which leads to a effective interparticle potential parameterized with single parameter,g [21], [35].

$$\begin{aligned}\Phi(\vec{r},t) &= \langle\hat{\Psi}(\vec{r}',t)\rangle \\ V(\vec{r},\vec{r}') &= g\delta(\vec{r}-\vec{r}')\end{aligned} \tag{2.5}$$

This approximation becomes exact at absolute zero, $T = 0K$.

Substituting Eq. (2.5) into Eq. (2.4), we get,

$$i\hbar\frac{\partial}{\partial t}\Phi(\vec{r},t) = \left[-\frac{\hbar^2}{2m}\bigtriangledown^2 + V_{ext}(\vec{r}) + g|\Phi(\vec{r},t)|^2\right]\Phi(\vec{r},t), \tag{2.6}$$

where g is called *the order parameter* for BEC and it is defined in terms of s-wave scattering length, a,

$$g = \frac{4\pi\hbar^2 a}{m}. \tag{2.7}$$

The evolution of the system is smooth. Hence, the time-dependent wavefunction is well behaved, since it is produced due to an effective potential. In addition, the energy variation with the total particle number, N, can be written as

$$\delta E - \mu\delta N = 0, \tag{2.8}$$

where μ is the chemical potential.

Therefore, the time-dependent wavefunction for the bosonic system with constant number of particle can be written as:

$$\Phi(\vec{r},t) = \phi(\vec{r})\exp\left(\frac{-i\mu t}{\hbar}\right) \tag{2.9}$$

Inserting Eq. (2.9) into Eq. (2.6).

$$\mu\phi(\vec{r}) = \left[-\frac{\hbar^2}{2m}\bigtriangledown^2 + V_{ext}(\vec{r}) + g|\phi(\vec{r})|^2\right]\phi(\vec{r}) \tag{2.10}$$

The wavefunction,ϕ can be chosen in the appropriate form for the following relations to hold:

$$N = \int d\vec{r}|\phi(\vec{r})|^2$$
$$n(\vec{r}) = |\phi(\vec{r})|^2 \tag{2.11}$$

Furthermore, the chemical potential is defined by Eq. (2.8) as:

$$\mu = \frac{\delta E}{\delta N} \tag{2.12}$$

Inserting Eq. (2.11) and Eq. (2.12) into Eq. (2.10), multiplying it with $\phi^*(\vec{r})$ and integrating the resulting equation over space, we obtain

$$E[n] = \int d\vec{r}\left(\frac{\hbar^2}{2m}|\bigtriangledown\sqrt{n}|^2 + V_{ext}(\vec{r})n + gn^2\right). \tag{2.13}$$

The Gross-Pitaevskii equation (Eq. (2.4)) provides an accurate description of the bosonic dilute gas in the ultracold regime.

Observation of BEC correspond to a phase transition in Bose gas. The interparticle interaction become insignificant in condense phase, while physical properties are determined via the interparticle interaction in the classical phase [17].

2.2.2 Fermions

In experimental works, the ultracold, dilute and harmonically trapped Fermi gases are composed of two different species of fermions or a Bose-Fermi mixture needed for the cooling precess. In this thesis and in the general accepted treatment in literature, only systems with identical fermions are studied.

This time, we start with the time-independent Hamiltonian in second quantization.

$$\begin{aligned}\hat{H} = &\int d\vec{r}\hat{\Psi}^{\dagger}(\vec{r})\left(-\frac{\hbar^2}{2m}\bigtriangledown^2 + V_{ext}(\vec{r})\right)\hat{\Psi}(\vec{r}) \\ &+ \frac{1}{2}\int d\vec{r}d\vec{r}'\hat{\Psi}^{\dagger}(\vec{r})\hat{\Psi}^{\dagger}(\vec{r}')V(\vec{r},\vec{r}')\hat{\Psi}(\vec{r}')\hat{\Psi}(\vec{r}),\end{aligned} \tag{2.14}$$

where $\hat{\Psi}^{\dagger}$ and $\hat{\Psi}$ are the fermion creation and annihilation fields operators respectively, defined as

$$\begin{aligned}\hat{\Psi}(\vec{r}) &= \sum_{\vec{k}}\psi_{\vec{k}}(\vec{r})a_{\vec{k}} \\ \hat{\Psi}^{\dagger}(\vec{r}) &= \sum_{\vec{k}}\psi^{\dagger}_{\vec{k}}(\vec{r})a^{\dagger}_{\vec{k}}\end{aligned} \tag{2.15}$$

where $a^{\dagger}_{\vec{k}}$ and $a^{\dagger}_{\vec{k}}$ are fermionic creation and annihilation operators and $\psi_{\vec{k}}$ is the single-particle wavefunction with the quantum number $\vec{k}$.

The Pauli exclusion principle forbids s-wave scattering and p-wave scattering contribution is small at the ultracold regime. Therefore, the significant interparticle interaction in Eq. (2.14) becomes the magnetic dipole-dipole (dd) interaction [8], [39].

$$V(\vec{r},\vec{r}') = V_{dd}(\vec{r},\vec{r}') = \frac{\mu_0\mu^2}{4\pi}\left(\frac{1}{|\vec{r}-\vec{r}'|^3} - \frac{3[\hat{\mu}\cdot(\vec{r}-\vec{r}')]^2}{|\vec{r}-\vec{r}'|^5}\right), \tag{2.16}$$

where μ_0 is the Bohr magneton, μ is the relative magnetic dipole moment of the fermionic atom and $\hat{\mu}$ represents the unit vector along the magnetic dipole at $\vec{r}$.

In the case of the harmonically trapped fermions, the external potential in Eq. (2.14) is the harmonic trap potential:

$$V_{ext}(\vec{r}) = V_{trap}(\vec{r}) = \frac{1}{2}m\left(\omega_x^2 x^2 + \omega_y^2 y^2 + \omega_z^2 z^2\right), \tag{2.17}$$

where m is the mass of the atom and ω_x, ω_y, ω_z are the angular frequencies of the applied fields along $\hat{x}$, $\hat{y}$, $\hat{z}$ respectively.

With these Eq. (2.14) can be written as

$$\begin{aligned}\hat{H} = &\int d\vec{r}\hat{\Psi}^\dagger(\vec{r})\left(-\frac{\hbar^2}{2m}\bigtriangledown^2 + \frac{1}{2}\left(\omega_x^2 x^+ \omega_y^2 y^2 + \omega_z^2 z^2\right)\right)\hat{\Psi}(\vec{r}) \\ &+ \frac{1}{2}\int d\vec{r}d\vec{r}'\hat{\Psi}^\dagger(\vec{r})\hat{\Psi}^\dagger(\vec{r}')\frac{\mu_0\mu^2}{4\pi}\left(\frac{1}{|\vec{r}-\vec{r}'|^3} - \frac{3[\hat{\mu}\cdot(\vec{r}-\vec{r}')]^2}{|\vec{r}-\vec{r}'|^5}\right)\hat{\Psi}(\vec{r}')\hat{\Psi}(\vec{r}).\end{aligned} \tag{2.18}$$

The ultracold regime limits cannot be applied to Eq. (2.18) unlike the bosonic case. The ultracold fermionic systems pose a great challenge to the many-body quantum theory. Therefore, many different methods are deployed to determine various properties of the ultracold, dilute Fermi gas.

2.2.2.1 The Variational Principle

In case that two-body interaction term introduces a positive contribution to the ground state energy, an upper bound for the latter can be determined for N-body fermionic system by using the variational principle [29]. The sign of the contribution coming from the dipolar term in Eq. (2.18) depends on the geometry of the system concidered and the geometry of the system can be controlled by applying desired trap potential. The variational principle is applicable for the systems for the appropriate geometries.

2.2.2.2 Thomas - Fermi - (Dirac) Approximation

In the study of Butts *et al.* [8], the Hamiltonian of the N spin polarized Fermi gas is approximated in terms of the single particle Hamiltonian with the assumption that the interparticle interaction can be neglected, if the interparticle distance exceeds the effective range of the interparticle interaction. This interaction has a short-range nature

and the Pauli exclusion principle leads to large interparticle distance compared the effective range of the interparticle interaction due to the Pauli pressure. This pressure causes repulsive force between fermions.

$$\hat{H} = \frac{\hbar}{2m}\left(k_x^2 + k_y^2 + k_z^2\right) + \frac{m\omega^2}{2}\left(x^2 + y^2 + \lambda z^2\right), \tag{2.19}$$

where m is mass, ω is the trap frequency and λ is the anisotropy constant.

The number density of particles in phase space for a system represented by Eq. (2.19) is written by TF (Thomas-Fermi) approximation as [40], [15]:

$$\rho(\vec{r}, \vec{k}) = \frac{1}{(2\pi)^3} \frac{1}{e^{\beta(E(\vec{r},\vec{k})-\mu)} + 1}, \tag{2.20}$$

where $E(\vec{r}, \vec{k})$ is the eigenvalue of the Hamiltonian in Eq. (2.19), μ is the chemical potential, $\beta = 1/k_B T$, k_B is the Boltzmann constant and T is temperature.

Integrating Eq. (2.20) over the phase space yields the total particle number as:

$$N = \int\int d^3r \; d^3p \; \rho(\vec{r}, \vec{k}), \tag{2.21}$$

and the density od particles in the system becomes

$$n(\vec{r}) = \frac{N}{V} = \int d^3p \; \rho(\vec{r}, \vec{k}). \tag{2.22}$$

At $T = 0$, the density becomes

$$n(\vec{r}) = \frac{k_F^3(\vec{r})}{6\pi^2}, \tag{2.23}$$

where $k_F(\vec{r})$ is the Fermi wavenumber at $\vec{r}$.

The interparticle interaction is the dipole-dipole interaction in Fermi gas. This ignored interaction in TF approximation is included in the works of Goral *et al.* in the scheme of Thomas-Fermi-Dirac (TFD) approximation [18]. The interparticle interaction in the trapped Fermi gas is the dipole-dipole interaction, $V_{dd}(\vec{r}, \vec{r'})$ and the energy contribution of this term is

$$E_{dd} = \int\int d^3r \; d^3r' \; V_{dd}(\vec{r}, \vec{r'}) n^{(2)}(\vec{r}, \vec{r'}) \tag{2.24}$$

where $n^{(2)}(\vec{r}, \vec{r'})$ is the two particles density matrix. Dirac (1930) proposed to approximate this two particles density matrix in terms of the single particle density in

Eq. (2.23) [13].

$$n^{(2)}(\vec{r},\vec{r'}) = n(\vec{r})n(\vec{r'}) + \Delta n^{(2)}(\vec{r},\vec{r'}), \tag{2.25}$$

where $n(\vec{r})n(\vec{r'})$ represents the direct energy in TFD approximation. In this approximation, the total energy is written as:

$$\begin{aligned} E[n] = \frac{\hbar^2}{2m}\int d^3r \left(\frac{1}{10\pi^2}(6\pi^2 n(\vec{r}))^{5/3} + m^2\omega^2 r^2 n(\vec{r})\right) \\ + \frac{1}{2}\int\int d^3r\ d^3r'\ n(\vec{r})V_{dd}(\vec{r},\vec{r'})n\vec{r'}) \end{aligned} \tag{2.26}$$

Goral *et al.* applied a energy minimization scheme to (2.26) to determine the density profile.

2.2.2.3 The Hartree-Fock (HF) Approximation

In the HF treatment of any fermionic system, the exchange term is reintroduced. The Hamiltonian in second quantization in terms of creation and annihilation operators is

$$\begin{aligned} \hat{H} = \sum_{\vec{k}}\left[\int d\vec{r}\psi^\dagger_{\vec{k}}(\vec{r})\left(-\frac{\hbar^2}{2m}\bigtriangledown^2 + \frac{1}{2}\left(\omega_x^2 x^+ \omega_y^2 y^2 + \omega_z^2 z^2\right)\right)\psi_{\vec{k}}(\vec{r})\right] a^\dagger_{\vec{k}} a_{\vec{k}} \\ + \frac{1}{2}\sum_{\vec{k}_1,\vec{k}_2,\vec{k}_3,\vec{k}_4}\left[\int d\vec{r}d\vec{r'}\psi^\dagger_{\vec{k}_1}(\vec{r})\psi^\dagger_{\vec{k}_2}(\vec{r'})\frac{\mu_0\mu^2}{4\pi}\left(\frac{1}{|\vec{r}-\vec{r'}|^3}\right.\right. \\ \left.\left. -\frac{3[\hat{\mu}(\vec{r}-\vec{r'})]^2}{|\vec{r}-\vec{r'}|^5}\right)\psi_{\vec{k}_4}(\vec{r'})\psi_{\vec{k}_3}(\vec{r})a^\dagger_{\vec{k}_1}a^\dagger_{\vec{k}_2}a_{\vec{k}_4}a_{\vec{k}_3} \end{aligned} \tag{2.27}$$

Writing Eq. (2.27) in more compact form.

$$\hat{H} = \sum_{\vec{k}}\tilde{T}_{\vec{k}}a^\dagger_{\vec{k}}a_{\vec{k}} + \frac{1}{2}\sum_{\vec{k}_1,\vec{k}_2,\vec{k}_3,\vec{k}_4}\tilde{V}_{\vec{k}_1,\vec{k}_2,\vec{k}_3,\vec{k}_4}a^\dagger_{\vec{k}_1}a^\dagger_{\vec{k}_2}a_{\vec{k}_4}a_{\vec{k}_3} \tag{2.28}$$

where $\tilde{T}_{\vec{k}}$ is the sum of the kinetic energy and the harmonic trap potential energy operators and $\tilde{V}_{\vec{k}_1,\vec{k}_2,\vec{k}_3,\vec{k}_4}$ is the dipole-dipole interaction operator in the second quantization for the specified $\vec{k}$ [16]. $\tilde{V}_{\vec{k}_1,\vec{k}_2,\vec{k}_3,\vec{k}_4}$ is a quartic operator. Evaluating the dipole-dipole interaction term in Eq. (2.28) by using the mean field decoupling [43].

$$\begin{aligned} \sum_{\vec{k}_1,\vec{k}_2,\vec{k}_3,\vec{k}_4}\tilde{V}_{\vec{k}_1,\vec{k}_2,\vec{k}_3,\vec{k}_4}a^\dagger_{\vec{k}_1}a^\dagger_{\vec{k}_2}a_{\vec{k}_3}a_{\vec{k}_4} = \sum_{\vec{k},\vec{k}'}\left[\left(V_H(\vec{k},\vec{k}') + V_F(\vec{k},\vec{k}')\right)a^\dagger_{\vec{k}'}a_{\vec{k}}\right. \\ - \frac{1}{2}\left(V_H(\vec{k},\vec{k}') + V_F(\vec{k},\vec{k}')\right)\langle a^\dagger_{\vec{k}'}a_{\vec{k}}\rangle - \frac{1}{2}\Delta(\vec{k},\vec{k}')\langle a^\dagger_{\vec{k}'}a^\dagger_{\vec{k}}\rangle \\ \left. + \frac{1}{2}\Delta(\vec{k},\vec{k}')a^\dagger_{\vec{k}'}a^\dagger_{\vec{k}} + \frac{1}{2}\Delta^\dagger(\vec{k},\vec{k}')a_{\vec{k}'}a_{\vec{k}}\right] \end{aligned} \tag{2.29}$$

where V_H is the Hartree term, V_F is the Fock term,Δ andΔ^* are the pairing term and its complex conjugate respectively.

$$
\begin{aligned}
V_H(\vec{k},\vec{k}') &= \sum_{\vec{s},\vec{s}'} \langle \vec{s}\vec{k}|V_{dd}|\vec{k}'\vec{s}'\rangle \langle a^\dagger_{\vec{s}} a_{\vec{s}'}\rangle \\
V_F(\vec{k},\vec{k}') &= \sum_{\vec{s},\vec{s}'} \langle \vec{s}\vec{k}|V_{dd}|\vec{s}'\vec{k}'\rangle \langle a^\dagger_{\vec{s}} a_{\vec{s}'}\rangle \\
\Delta(\vec{k},\vec{k}') &= \sum_{\vec{s},\vec{s}'} \langle \vec{k}\vec{k}'|V_{dd}|\vec{s}\vec{s}'\rangle \langle a_{\vec{s}} a_{\vec{s}'}\rangle
\end{aligned}
\tag{2.30}
$$

where $|\vec{k}\rangle$ represents the single-particle wavefunction,$\psi_{\vec{k}}(\vec{r})$ and the atomic orbitals are used in the HF approximation.

By the HF approximation, the distortion in the momentum Fermi surface caused by the Fock term and the superfluid pairing phenomena can be shown under the assumption of the pairing occurrence only between $(\vec{k}, -\vec{k})$ duals.

2.3 Density Functional Theory

Quantum mechanics was groundbreaking in understanding physical phenomena at the microscopic scale. *In principle*, it provides quite complete and consistent descriptions of systems and their dynamics. Typically, systems at the microscopic scale consist of a large number of particles. However, exact quantum mechanical solutions can be found only for a very limited number of small or noninteracting systems. Many approximation methods have been developed to overcome this constraint.

Density Functional Theory (DFT) is a density based method to many-body problems in quantum mechanics. It has received increasing attention in the last decades as a result of ever increasing computational power.

2.3.1 Historical Development

In quantum mechanics, the primary purpose is to solve the Schrödinger equation for the given system and find its wavefunction.

$$
i\hbar^2 \frac{\partial}{\partial t}\Psi = \hat{H}\Psi \tag{2.31}
$$

where $\Psi = \Psi(\vec{x}_1, \vec{x}_2, ...)$ and $\vec{x}_i = (\vec{r}_i, \sigma_i)$. Here $\vec{r}_i$ is the spatial and σ_i is the spin coordinate of particle i. $\hat{H}$ is the many-body Hamiltonian of the system.

In this thesis, only the time-independent case will be considered. Hence, the wavefunction will be assumed to be time-independent, which reduces the time-dependent Schrödinger equation to an eigenvalue problem.

$$\hat{H}\Psi = E\Psi \tag{2.32}$$

where E is the energy eigenvalue corresponding to Ψ.

For a system of N particles, the wavefunction is a function of $4N$ variables, $3N$ from the spatial coordinates of particles and N from their spin properties. Solving Eq.(2.32) is quite challenging even for simple cases and impossible for N greater than 2.

The first use of density rather than wavefunction belongs to Llewellyn Thomas and Enrico Fermi in 1927, in the early stage of quantum mechanics. Their method is referred to as Thomas-Fermi (TF) approximation [33].

In TF approximation, the many-body kinetic energy term is written as functional of density by considering an ideal uniform electron gas and assuming spin degeneracy.

$$T_{TF}[n(\vec{r})] = \frac{3^{5/3}\pi^{4/3}}{10} \int d\vec{r} n^{5/3}(\vec{r}) \tag{2.33}$$

Other terms in many-body Hamiltonian are treated in classically. The Thomas-Fermi approximation uses the classical Coulombic potential to include electron-electron interaction in Hamiltonian.

$$\hat{H} = \frac{3^{5/3}\pi^{4/3}}{10} \int d\vec{r} n^{5/3}(\vec{r}) + \int d\vec{r} v_{ext}(\vec{r}) n(\vec{r}) + \frac{1}{2} \int \int d\vec{r} d\vec{r}' \frac{n(\vec{r}) n(\vec{r}')}{|\vec{r} - \vec{r}'|} \tag{2.34}$$

Even though the TF model and DFT is theoretically different, TF approximation can be regarded as ancestor of DFT from a conceptual point of view.

2.3.2 The Many-Body Hamiltonian and Energy Functional

Quantum mechanical description of a system can be made with its Hamiltonian.

$$\begin{aligned}\hat{H} &= \hat{T} + \hat{V} \\ &= \hat{T} + \hat{V}_{ext} + \hat{V}_{int}\end{aligned} \tag{2.35}$$

where $\hat{T}$ and $\hat{V}$ are time-independent kinetic energy and potential energy operators in the Schrödinger picture.

In the interacting case, the potential operator contains the internal potential energy operator, $\hat{V}_{int}$ and external potential energy operator, $\hat{V}_{ext}$. $\hat{V}_{int}$ contains interparticle interaction terms and $\hat{V}_{ext}$ is a single particle operator including any kind of interactions of particles with an external potential. $\hat{T}$ is the many-body particle kinetic energy operator.

Disregarding spin polarization for simplicity, the Hamiltonian of N interacting and identical particle can be represented as:

$$\hat{H} = -\frac{\hbar^2}{2m}\sum_{i=1}^{N} \nabla_i^2 + \frac{1}{2}\sum_{i=1}^{N}\sum_{i\neq j=1}^{N} \hat{V}(\vec{r}_i, \vec{r}_j) + \sum_{i=1}^{N} \hat{V}_{ext}(\vec{r}_i) \tag{2.36}$$

with the total energy of the system

$$E = \langle \Psi | \hat{H} | \Psi \rangle \tag{2.37}$$

Due to difficulty of finding Ψ, DFT proposes to shift the focus to the density. Density can be defined by the density operator:

$$\hat{n}(\vec{r}) = \sum_{i=1}^{N} \delta^3(\vec{r} - \vec{r}_i), \tag{2.38}$$

With this definition, the density for any $\vec{r}$ be expressed as

$$\begin{aligned}n(\vec{r}) &= \langle \Psi | \hat{n}(\vec{r}) | \Psi \rangle \\ &= \sum_{i=1}^{N} \int d\vec{r}_1 ... d\vec{r}_N \delta^3(\vec{r} - \vec{r}_i) |\Psi(\vec{r}_1, ..., \vec{r}_N)|^2 \\ &= \sum_{i=1}^{N} \int d\vec{r}_1 ... d\vec{r}_{i-1} d\vec{r}_{i+1} ... d\vec{r}_N |\Psi(\vec{r}_1, ..., \vec{r}_{i-1}, \vec{r}, \vec{r}_{i+1}, ..., \vec{r}_N)|^2\end{aligned} \tag{2.39}$$

There are N identical integrals in Eq. (2.39) due to sum over positions of particles.

$$n(\vec{r}) = N \int d\vec{r}_2 ... d\vec{r}_N |\Psi(\vec{r}, \vec{r}_2, ..., \vec{r}_N)|^2 \tag{2.40}$$

Naturally, density is normalized to total particle number.

$$\int_V d\vec{r} n(\vec{r}) = N \tag{2.41}$$

A similar derivation yields the two particle density,

$$n(\vec{r}, \vec{r'}) = N(N-1) \int d\vec{r}_3 ... d\vec{r}_N |\Psi(\vec{r}, \vec{r}', \vec{r}_3, ..., \vec{r}_N|^2 \tag{2.42}$$

Let us recall Eq. (2.37) and inserting Eq. (2.36) into Eq. (2.37)

$$\begin{aligned} E &= \langle \Psi | \hat{H} | \Psi \rangle \\ &= \langle \Psi(\vec{r}_1, ..., \vec{r}_N)| - \frac{\hbar^2}{2m} \sum_{i=1}^{N} \nabla_i^2 + \frac{1}{2} \sum_{i=1}^{N} \sum_{i \neq j=1}^{N} \hat{V}(\vec{r}_i, \vec{r}_j) \\ &\quad + \sum_{i=1}^{N} \hat{V}_{ext}(\vec{r}_i) | \Psi(\vec{r}_1, ..., \vec{r}_N) \rangle \end{aligned} \tag{2.43}$$

The total energy, E can be written as the summation of the expectation values of each term in Eq. (2.43).

$$\begin{aligned} E &= -\frac{\hbar^2}{2m} \sum_{i=1}^{N} \langle \Psi(\vec{r}_1, ..., \vec{r}_N)| \nabla_i^2 |\Psi(\vec{r}_1, ..., \vec{r}_N) \rangle \\ &\quad + \frac{1}{2} \sum_{i=1}^{N} \sum_{i \neq j=1}^{N} \langle \Psi(\vec{r}_1, ..., \vec{r}_N) | \hat{V}(\vec{r}_i, \vec{r}_j) | \Psi(\vec{r}_1, ..., \vec{r}_N) \rangle \\ &\quad + \sum_{i=1}^{N} \langle \Psi(\vec{r}_1, ..., \vec{r}_N) | \hat{V}_{ext}(\vec{r}_i) | \Psi(\vec{r}_1, ..., \vec{r}_N) \rangle \\ &= T + E_{pp} + E_{ext} \end{aligned} \tag{2.44}$$

where T is the many-body kinetic energy, E_{pp} is the two-particle interaction energy and E_{ext} is the particle-external potential interaction energy.

Let us deal each term in Eq.(2.43) separately starting with the second term, since, the kinetic energy term needs special treatment to evaluate. Assuming that the two-body

term does not include any derivatives , it can be evaluated as:

$$\sum_{i=1}^{N}\sum_{i\neq j=1}^{N}\langle\Psi(\vec{r}_1,...,\vec{r}_N)|\hat{V}(\vec{r}_i,\vec{r}_j)|\Psi(\vec{r}_1,...,\vec{r}_N)\rangle$$
$$=\sum_{i=1}^{N}\sum_{i\neq j=1}^{N}\int d\vec{r}_1...d\vec{r}_N\Psi^*(\vec{r}_1,...,\vec{r}_N)V(\vec{r}_i,\vec{r}_j)\Psi(\vec{r}_1,...,\vec{r}_N)$$
$$=\sum_{i=1}^{N}\sum_{i\neq j=1}^{N}\int\int d\vec{r}_i d\vec{r}_j V(\vec{r}_i,\vec{r}_j)$$
$$\times\int d\vec{r}_1...d\vec{r}_{i-1}...d\vec{r}_{i+1}d\vec{r}_{j-1}d\vec{r}_{j+1}...d\vec{r}_N|\Psi(\vec{r}_1,...,\vec{r}_N)|^2 \tag{2.45}$$

There are $N(N-1)$ identical integrals in Eq. (2.45), since the norm of wavefunction is in concern.

$$\sum_{i=1}^{N}\sum_{i\neq j=1}^{N}\langle\Psi(\vec{r}_1,...,\vec{r}_N)|\hat{V}(\vec{r}_i,\vec{r}_j)|\Psi(\vec{r}_1,...,\vec{r}_N)\rangle=\int\int d\vec{r}d\vec{r}'V(\vec{r},\vec{r}')$$
$$\times\int d\vec{r}_3...d\vec{r}_N|\Psi(\vec{r},\vec{r}',\vec{r}_3,...,\vec{r}_N)|^2 \tag{2.46}$$

Inserting Eq. (2.42) into Eq. (2.46)

$$\sum_{i=1}^{N}\sum_{i\neq j=1}^{N}\langle\Psi(\vec{r}_1,...,\vec{r}_N)|\hat{V}(\vec{r}_i,\vec{r}_j)|\Psi(\vec{r}_1,...,\vec{r}_N)\rangle=\int\int d\vec{r}d\vec{r}'V(\vec{r},\vec{r}')n(\vec{r},\vec{r'}) \tag{2.47}$$

The two-body density represents the probability of existence of density at $\vec{r}$ in the presence of the probability of existence of density at $\vec{r}'$. DFT makes use of the expression of the particle energy in terms of the single particle density. For this reason, an approximation in terms of single-body densities is needed. The two-body density is written to the two-body density in terms of single particle density of uncorrelated systems with a correction part to encounter correlation later.

$$n(\vec{r},\vec{r'})=n(\vec{r})n(\vec{r}')+\Delta n(\vec{r},\vec{r'}) \tag{2.48}$$

With this representation, energy functional of particle-particle interaction is stated as:

$$E_{pp}[n]=\int\int d\vec{r}d\vec{r}'V(\vec{r},\vec{r}')n(\vec{r})n(\vec{r'})+\Delta E_{pp} \tag{2.49}$$

The additional term in Eq. (2.49) is correction due to single-body density approximation to two-body density.

Using similar argument, the energy function for interaction of particle with the external potential can be derived under assumption that external potential does not contain any derivative.

$$\sum_{i=1}^{N} \langle \Psi(\vec{r}_1, ..., \vec{r}_N) | \hat{V}_{ext}(\vec{r}_i) | \Psi(\vec{r}_1, ..., \vec{r}_N) \rangle$$
$$= \sum_{i=1}^{N} \int d\vec{r}_1 ... d\vec{r}_N \Psi^*(\vec{r}_1, ..., \vec{r}_N) V_{ext}(\vec{r}_i) \Psi(\vec{r}_1, ..., \vec{r}_N) \tag{2.50}$$

Since each integral is over all the volume, N identical integrals exist in Eq. (2.50) due to sum over particles and (2.50) becomes:

$$N \int d\vec{r} V_{ext}(\vec{r}) \int d\vec{r}_2 ... d\vec{r}_N |\Psi(\vec{r}, \vec{r}_2, ..., \vec{r}_N)|^2 \tag{2.51}$$

Inserting Eq. (2.40) into Eq. (2.51), one obtains

$$E_{ext}[n] = \int d\vec{r} V_{ext}(\vec{r}) n(\vec{r}) \tag{2.52}$$

Even though using density as the main variable seems convenient, the kinetic energy term cannot directly be written in terms of the density, since it contains second order partial derivative of spatial coordinates. Hence, there needs special treatment. The kinetic energy term will be abandoned for now. It will discussed in further section after introducing basis of DFT for sticking to historical process of theory.

2.3.3 The Hohenberg-Kohn Theorems

Even though the concept of using density instead of multi-variable wavefunction is relatively older, the backbone of DFT was constructed by Hohenberg and Kohn in 1964. [24] Two strong and crucial theorems known as Hohenberg-Kohn theorems are stated and proven in their work.

2.3.3.1 First Hohenberg-Kohn Theorem: Proof of Existence

The density of interacting particles, $n(\vec{r})$ in an external potential, $V_{ext}(\vec{r})$, is determined uniquely for $V_{ext}(\vec{r})$. Conversely, the density of interacting particle, $n(\vec{r})$ cor-

responds to an external potential, $V_{ext}(\vec{r})$ uniquely.

Proof:

Assume that the ground state of the system considered is not degenerate, and there are two separate external potentials, $V_{ext}(\vec{r})$ and $V'_{ext}(\vec{r})$ corresponding to the same density, $n_0(\vec{r})$. Since the external potentials are distinct, the Hamiltonian operators, $\hat{H}$ and $\hat{H}'$, and their ground state wavefunctions, Ψ and Ψ' are also distinct.

By the variation principle, the following inequalities can be written:

$$\begin{aligned} E &= \langle\Psi|H|\Psi\rangle < \langle\Psi'|H|\Psi'\rangle \\ E' &= \langle\Psi'|H'|\Psi'\rangle < \langle\Psi|H'|\Psi\rangle \end{aligned} \tag{2.53}$$

Adding the identities in Eq. (2.53) yield the inequality.

$$E + E' < \langle\Psi'|\hat{H}|\Psi'\rangle + \langle\Psi|\hat{H}'|\Psi\rangle \tag{2.54}$$

The kinetic energy operator and interparticle potential are common in both. These sum of these two terms $universal$ and is generally labeled as $\hat{F}$. Through the universal functional, F and the ground state density, $n_0(\vec{r})$ are common. The total energy functional for H' can be written as:

$$\langle\Psi|\hat{H}'|\Psi\rangle = \langle\Psi|\hat{F}|\Psi\rangle + \int d\vec{r}V'_{ext}(\vec{r})n_0(\vec{r}) \tag{2.55}$$

Adding and subtracting a term into Eq. (2.55) yields.

$$\begin{aligned} \langle\Psi|H'|\Psi\rangle &= \langle\Psi|F|\Psi\rangle + \int d\vec{r}V'_{ext}(\vec{r})n_0(\vec{r}) \\ &\quad + \int d\vec{r}V_{ext}(\vec{r})n_0(\vec{r}) - \int d\vec{r}V_{ext}(\vec{r})n_0(\vec{r}) \\ &= \langle\Psi|H|\Psi\rangle + \int d\vec{r}V'_{ext}(\vec{r})n_0(\vec{r}) - \int d\vec{r}V_{ext}(\vec{r})n_0(\vec{r}) \end{aligned} \tag{2.56}$$

Similarly,

$$\langle\Psi'|H|\Psi'\rangle = \langle\Psi'|H'|\Psi'\rangle + \int d\vec{r}V_{ext}(\vec{r})n_0(\vec{r}) - \int d\vec{r}V'_{ext}(\vec{r})n_0(\vec{r}) \tag{2.57}$$

By adding Eq. (2.56) and Eq. (2.57):

$$\langle\Psi'|H|\Psi'\rangle + \langle\Psi|H'|\Psi\rangle = E + E' \tag{2.58}$$

Inserting Eq. (2.58) into Eq. (2.54):

$$E + E' < E + E' \tag{2.59}$$

which is contradictory and by *reductio ad absurdum*, the first Hohenberg-Kohn theorem is proven.

2.3.3.2 Second Hohenberg-Kohn Theorem: Variational Principle

If the ground state of a system is not degenerate, then the corresponding energy functional, $E[n(\vec{r})]$ for any density, $n(\vec{r})$ is greater than or equal to the ground state energy, E_0.

$$E[n(\vec{r})] \geq E_0 \tag{2.60}$$

Proof: Since the ground state is not degenerate, than there is a ground state density, $n_0(\vec{r})$, which determines the external potential uniquely by the first Hohenberg-Kohn theorem. Hence, the ground state energy functional can be written uniquely.

$$E_0 = E[n_0] = F[n_0] + \int d\vec{r} V_{ext}(\vec{r}) n_0(\vec{r}) \tag{2.61}$$

where $F[n_0]$ is the universal functional.

Furthermore, the ground state density determines the ground state wavefunction, Ψ_0. By the variational principle, the following inequality can be written for any wavefunction:

$$E_0 = E[n_0] = \langle \Psi_0 | H | \Psi_0 \rangle \leq \langle \Psi | H | \Psi \rangle = E[n] \tag{2.62}$$

which proves Eq. (2.60).

2.3.4 The Kohn-Sham Method

Following the proof of principle by Hohenberg and Kohn, Kohn and Sham published an article dealing with the practical implementation [28].

The core ansatz in the Kohn-Sham (KS) method is that density can be written as sum of square of some orbitals.

$$n(\vec{r}) = \sum_{i=1}^{N} |\phi_i(\vec{r})|^2 \tag{2.63}$$

The Kohn - Sham orbitals are purely mathematical functions, which satisfy Eq. (2.63). The physical meaning of the KS orbitals is controversial and still debated over [38].

The true kinetic energy can be broken down into the single-particle kinetic energy obtained by using KS orbitals and a correction.

$$\begin{aligned} &-\frac{\hbar^2}{2m}\sum_{i=1}^{N}\langle\Psi(\vec{r}_1,...,\vec{r}_N)|\bigtriangledown_i^2|\Psi(\vec{r}_1,...,\vec{r}_N)\rangle \\ &\quad = -\frac{\hbar^2}{2m}\sum_{i=1}^{N}\int d\vec{r}_i\Psi^*(\vec{r}_1,...,\vec{r}_N)\bigtriangledown_i^2\Psi(\vec{r}_1,...,\vec{r}_N) \\ &\quad = -\frac{\hbar^2}{2m}\sum_{i=1}^{N}\int d\vec{r}\phi_i^*(\vec{r})\bigtriangledown^2\phi_i(\vec{r}) + \Delta T \end{aligned} \tag{2.64}$$

With this, E can be written as a functional of the density.

$$\begin{aligned} E[n] &= T[n] + E_{pp}[n] + E_{ext}[n] + \Delta T + \Delta E_{pp} \\ &= -\frac{\hbar^2}{2m}\sum_{i=1}^{N}\int d\vec{r}\phi_i^*(\vec{r})\bigtriangledown^2\phi_i(\vec{r}) + \frac{1}{2}\int\int d\vec{r}d\vec{r}'V_H(\vec{r},\vec{r}')n(\vec{r})n(\vec{r'}) \\ &\quad + \int d\vec{r}V_{ext}(\vec{r})n(\vec{r}) + \Delta T + \Delta E_{pp} \end{aligned} \tag{2.65}$$

where $V_{ext}(\vec{r})$ is called *the external potential* and $V_H(\vec{r},\vec{r}')$ is called *the Hartree potential*, which is the classical part of the interparticle interaction energy.

Renaming corrections to kinetic energy functional and two-body interaction energy function as $E_{xc} = \Delta T + \Delta E_{pp}$, which is called *exchange-correlation energy* in total.

$$\begin{aligned} E[n] = &-\frac{\hbar^2}{2m}\sum_{i=1}^{N}\int d\vec{r}\phi_i^*(\vec{r})\bigtriangledown^2\phi_i(\vec{r}) + \frac{1}{2}\int\int d\vec{r}d\vec{r}'V_H(\vec{r},\vec{r}')n(\vec{r})n(\vec{r'}) \\ &+ \int d\vec{r}V_{ext}(\vec{r})n(\vec{r}) + E_{xc} \end{aligned} \tag{2.66}$$

Many approximation methods exist in literature for E_{xc}. The oldest and one of the most commonly used approximation is Local Density Approximation (LDA), where

E_{xc} is derived from the exchange-correlation energy of the homogeneous particle gas [27].

$$E_{xc}^{LDA} = \int d\vec{r}\epsilon_{xc}[n]n(\vec{r}) \tag{2.67}$$

Inserting Eq.(2.67) into Eq.(2.66) and performing a functional differentiation it with respect to $\phi^*(\vec{r})$.

$$\begin{aligned}\frac{\delta E[n]}{\delta \phi_i^*} = \Bigg(-\frac{\hbar^2}{2m}\bigtriangledown^2 + \int d\vec{r}' V_H(\vec{r},\vec{r}')n(\vec{r}) \\ +V_{ext}(\vec{r}) + \epsilon_{xc}[n] + n(\vec{r})\frac{\delta\epsilon_{xc}[n]}{\delta n}\Bigg)\phi_i = \varepsilon_i\phi_i\end{aligned} \tag{2.68}$$

which can be written as

$$[T + V_{eff}]\phi_i = \varepsilon_i\phi_i \tag{2.69}$$

The system of equations are referred to as Kohn-Sham equations. The sum of the eigenvalues can be related by multiplying Eq.(2.68) KS equation by ϕ_i^* from the left, integrating over volume and summing over i.

$$\begin{aligned}\sum_{i=1}^{N}\int d\vec{r}\phi_i^*(\vec{r})\Bigg(-\frac{\hbar^2}{2m}\bigtriangledown^2 + \int d\vec{r}' V_H(\vec{r},\vec{r}')n(\vec{r}) \\ +V_{ext}(\vec{r}) + \epsilon_{xc}[n] + n(\vec{r})\frac{\delta\epsilon_{xc}[n]}{\delta n}\Bigg)\phi_i(\vec{r}) = \sum_{i=1}^{N}\varepsilon_i\end{aligned} \tag{2.70}$$

Changing orders of summation and integral and inserting Eq. (2.63).

$$\begin{aligned}\sum_{i=1}^{N}\varepsilon_i = -\frac{\hbar^2}{2m}\sum_{i=1}^{N}\int d\vec{r}\phi_i^*(\vec{r})\bigtriangledown^2\phi_i(\vec{r}) + \int\int d\vec{r}d\vec{r}' V(\vec{r},\vec{r}')n(\vec{r})n(\vec{r}') \\ + \int d\vec{r}V_{ext}(\vec{r})n(\vec{r}) + \int d\vec{r}\epsilon_{xc}[n]n(\vec{r}) + \int d\vec{r}n^2(\vec{r})\frac{\delta\epsilon_{xc}[n]}{\delta n}\end{aligned} \tag{2.71}$$

The difference between the sum of KS energies and the true energy, ΔE can be found by subtracting Eq. (2.71) from Eq. (2.66).

$$\begin{aligned}\Delta E &= E[n] - \sum_{i=1}^{N}\varepsilon_i \\ &= -\frac{1}{2}E_{pp}[n] - \int d\vec{r}n^2(\vec{r})\frac{\delta\epsilon_{xc}[n]}{\delta n}\end{aligned} \tag{2.72}$$

Due to the highly nonlinear nature of the problem with V_{eff} dependent on the KS orbitals, the system of equations in Eq.(2.69) must be solved self-consistently. This may be achieved by a suitable initial guess for the density and subsequent iterations until convergence reached.

CHAPTER 3

THE DIPOLAR FERMI GAS

The ultracold, dilute Fermi gas under the harmonic trap will be explored by using Density Functional Theory (DFT). Starting from the many-body Hamiltonian of the system, Kohn-Sham equations are derived with a suitable exchange functional.

3.1 The Model

The many-body Hamiltonian of the dipolar Fermi gas subject to a trap is expressed in the International System of Units (SI) as

$$\begin{aligned}\hat{H} &= \hat{T} + \hat{V}_{trap} + \hat{V}_{dd} \\ &= -\frac{\hbar^2}{2m}\sum_i^N \nabla_i^2 + \frac{1}{2}m\sum_i^N \left(\omega_x^2 x_i^2 + \omega_y^2 y_i^2 + \omega_z^2 z_i^2\right) \\ &\quad + \frac{1}{2}\frac{\mu_0\mu^2}{4\pi}\sum_i^N\sum_{j\neq i}^N \left(\frac{1}{|\vec{r}_i - \vec{r}_j|^3} - \frac{3[\hat{\mu}\cdot(\vec{r}_i - \vec{r}_j)]^2}{|\vec{r}_i - \vec{r}_j|^5}\right)\end{aligned} \tag{3.1}$$

where N is the number of particles, $\vec{\mu}$ is the magnetic dipole moment and $\omega_x, \omega_y, \omega_z$ define the geometry of the confining trap.

In an experimental setup, the desired harmonic trap can be created by using lasers in an appropriate geometry and frequencies. In the most general case as defined in Eq. (3.1), the trap is allowed to be anisotropic. However, in this thesis we assume a completely isotropic trap with $\omega_x = \omega_y = \omega_z = \omega$.

With this assumption, the trap potential becomes

$$\hat{V}_{trap} = \frac{1}{2} m\omega^2 \sum_i^N r_i^2, \tag{3.2}$$

where $\vec{r}_i = x_i\hat{i} + y_i\hat{j} + z_i\hat{k}$.

Next, we assume that the magnetic dipoles are aligned along the same direction with the help of a small external magnetic field. This scenario can be realized in experiments [1], [20], [32], [12].

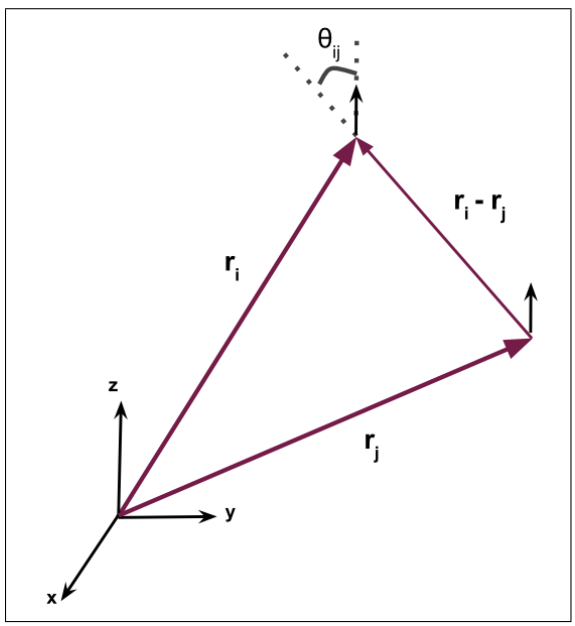

Figure 3.1: Schematic definition of the angle θ_{ij}

Taking the z-axis to lie parallel to the magnetic moment, we define the angle between the z-axis and the difference vector $\vec{r}_i - \vec{r}_j$ between the ith and j^{th} dipoles as θ_{ij}. A schematic depiction of this setup can be seen in Fig. 3.1.

The dipole-dipole interaction operator then reduces to the simple form

$$\hat{V}_{dd} = \frac{\mu_0\mu^2}{4\pi} \sum_i^N \sum_{j\neq i}^N \frac{1 - 3\cos^2\theta_{ij}}{|\vec{r}_i - \vec{r}_j|^3}, \tag{3.3}$$

With these simplifications, Eq. (3.1) becomes,

$$\hat{H} = -\frac{\hbar^2}{2m} \sum_i^N \nabla_i^2 + \frac{1}{2} m\omega^2 \sum_i^N r_i^2 + \frac{1}{2} \frac{\mu_0\mu^2}{4\pi} \sum_i^N \sum_{j\neq i}^N \frac{1 - 3\cos^2\theta_{ij}}{|\vec{r}_i - \vec{r}_j|^3} \tag{3.4}$$

3.2 Rescaling the Hamiltonian

In order to simplify Eq. (3.4), we rescale all lengths by the harmonic length $l = \sqrt{\frac{\hbar}{m\omega}}$, while all energies are expressed in terms of $\hbar\omega$. This leads to the following transformation

$$\begin{aligned} r_i &\to \frac{r_i}{l} = \sqrt{\frac{m\omega}{\hbar}} r_i \\ \hat{H} &\to \frac{\hat{H}}{\hbar\omega} \end{aligned} \tag{3.5}$$

which converts Eq. (3.4) into a simpler form.

$$\begin{aligned} \hat{H} = \frac{1}{\hbar\omega} \Bigg[& \frac{m\omega}{\hbar} \left(-\frac{\hbar^2}{2m} \sum_i^N \nabla_i^2 \right) + \frac{\hbar}{m\omega} \left(\frac{1}{2} m\omega^2 \sum_i^N r_i^2 \right) \\ & + \left(\frac{m\omega}{\hbar} \right)^{3/2} \left(\frac{\mu_0 \mu^2}{8\pi} \sum_i^N \sum_{j \neq i}^N \frac{1 - 3\cos^2\theta_{ij}}{|\vec{r}_i - \vec{r}_j|^3} \right) \Bigg] \end{aligned} \tag{3.6}$$

Simplifying Eq. (3.6) yields the dimensionless Hamiltonian as

$$\hat{H} = -\frac{1}{2} \sum_i^N \nabla_i^2 + \frac{1}{2} \sum_i^N r_i^2 + \frac{1}{2} g \sum_i^N \sum_{j \neq i}^N \frac{1 - 3\cos^2\theta_{ij}}{|\vec{r}_i - \vec{r}_j|^3}, \tag{3.7}$$

where g parameterizes the interaction of the whole system with respect to the frequency of the harmonic trap, ω, the mass, m, and the intrinsic magnetic moment, μ, of the fermion.

$$g = \frac{\mu_0 \mu^2}{4\pi l^3 \hbar\omega}. \tag{3.8}$$

3.3 The Kohn-Sham Orbitals

The definition of the density in terms of the KS orbitals is expressed as follows.

$$n(\vec{r}) = \sum_{i=0}^{\infty} n_i |\phi_i(\vec{r})|^2 \tag{3.9}$$

where $\{n_i\}$ are the occupations of the KS orbital. At $T = 0$, $n_0, n_1, ..., n_N$ is 1, while $n_{N+1}, ..., n_\infty$ are all 0.

The KS equation for the system introduced by recalling Eq. (2.68) with the LDA exchange-correlation functional is

$$\left(-\frac{1}{2}\nabla^2 + \frac{1}{2}r^2 + g\int d^3r' \frac{1-3\cos^2\theta_{\vec{r}\vec{r}'}}{|\vec{r}-\vec{r}'|^3} n(\vec{r}') + \epsilon_{xc} + n(\vec{r}')\frac{d\epsilon_{xc}}{dn})\right)\phi_i(\vec{r}) = \varepsilon_i\phi_i(\vec{r}) \tag{3.10}$$

where $\theta_{\vec{r}\vec{r}'}$ represents the angle between $\vec{r}-\vec{r}'$ and z-axis .

The terms in parenthesis may be redefined as an effective Hamiltonian which allows (3.10) to be written in a more compact form:

$$\hat{H}_{eff}\phi_i = \varepsilon_i\phi_i. \tag{3.11}$$

Expanding each KS orbital in terms of the chosen, orthogonal basis functions leads to

$$\phi_i(\vec{r}) = \sum_j^{N_B} c_{ij}\psi_j(\vec{r}), \tag{3.12}$$

where N_B is the number of basis functions. Although, N_B should be infinite for an exact expansion of the KS orbitals, for practical calculations N_B is chosen to be a number somewhat larger than N. In addition, the basis functions satisfy the orthonormality property,

$$\int d^3r\psi_i(\vec{r})\psi_j(\vec{r}) = \delta_{ij}. \tag{3.13}$$

Inserting Eq. (3.12) into Eq. (3.10) yields

$$\sum_j^{N_B}\hat{H}_{eff}c_{ij}\psi_j(\vec{r}) = \varepsilon_i\sum_j^{N_B}c_{ij}\psi_j(\vec{r}). \tag{3.14}$$

Multiplying Eq. (3.14) by $\psi_k(\vec{r})$ and integrating over the volume, we obtain

$$\sum_j^{N_B}c_{ij}\int d^3r\psi_k(\vec{r})\hat{H}_{eff}\psi_j(\vec{r}) = \varepsilon_i\sum_j^{N_B}c_{ij}\int d^3r\psi_k(\vec{r})\psi_j(\vec{r}). \tag{3.15}$$

Eq. (3.15) may be reexpressed by inducing the condition in Eq. (3.13) as

$$\sum_j^{N_B}c_{ij}\int d^3r\psi_k(\vec{r})\hat{H}_{eff}\psi_j(\vec{r}) = \varepsilon_i c_{ik}, \tag{3.16}$$

which can be expressed in Dirac notation as

$$.\sum_j^{N_B}c_{ij}\langle\psi_k|\hat{H}_{eff}|\psi_j\rangle = \varepsilon_i c_{ik} \tag{3.17}$$

Eq. (3.17) can now be expressed in a matrix equation form:

$$\begin{pmatrix} \langle\psi_1|\hat{H}_{eff}|\psi_1\rangle & \cdots & \langle\psi_1|\hat{H}_{eff}|\psi_{NB}\rangle \\ \langle\psi_2|\hat{H}_{eff}|\psi_1\rangle & \cdots & \langle\psi_1|\hat{H}_{eff}|\psi_{NB}\rangle \\ \vdots & \ddots & \vdots \\ \langle\psi_{NB}|\hat{H}_{eff}|\psi_1\rangle & \cdot & \langle\psi_{NB}|\hat{H}_{eff}|\psi_{NB}\rangle \end{pmatrix} \begin{pmatrix} c_1 \\ c_2 \\ \vdots \\ c_{NB} \end{pmatrix} = \varepsilon \begin{pmatrix} c_1 \\ c_2 \\ \vdots \\ c_{NB} \end{pmatrix} \tag{3.18}$$

Finally Eq. (3.18) may be written in a compact form as

$$\bar{H}\bar{C} = \varepsilon\bar{C}. \tag{3.19}$$

By this process, the second order partial differential equation in Eq. (3.10) reduces to the matrix equation in Eq. (3.19). Eq. (3.19) is solved by the matrix diagonalization methods [9].

3.3.1 The Basis Functions

The choice of the basis functions used in expanding the KS orbitals are completely arbitrary as long as the basis functions satisfy the orthogonality condition in Eq. (3.12). The ij-th element of the effective Hamiltonian matrix is

$$H_{ij} = \langle\psi_i|\hat{H}_{eff}|\psi_j\rangle = \langle\psi_i|\hat{T} + \hat{V}_{trap} + \hat{V}_{dd} + \hat{V}_{xc}|\psi_j\rangle. \tag{3.20}$$

Our choice for the basis functions are motivated by the fact that $\hat{T} + \hat{V}_{trap}$ is the Hamiltonian of a system of non-interacting particles in a three dimensional isotropic harmonic oscillators. In other words,

$$\hat{H}_{ho} = \hat{T} + \hat{V}_{trap} = -\frac{1}{2}\nabla^2 + \frac{1}{2}r^2, \tag{3.21}$$

Therefore, using the eigenfunctions of the $\hat{H}_{ho}$ as the basis functions reduces the number of calculations necessary.

The isotropy of the harmonic trap potential allow us to use the spherical coordinates.

$$\left(-\frac{1}{2}\nabla^2 + \frac{1}{2}r^2\right)\psi(r,\theta,\varphi) = E\psi(r,\theta,\varphi). \tag{3.22}$$

where the Laplacian operator in spherical coordinate is

$$\begin{aligned}\nabla^2 &= \frac{1}{r^2}\frac{\partial}{\partial r}\left(r^2\frac{\partial}{\partial r}\right) + \frac{1}{r^2\sin\theta}\frac{\partial}{\partial\theta}\left(\sin\theta\frac{\partial}{\partial\theta}\right) + \frac{1}{\sin^2\theta}\frac{\partial^2}{\partial\varphi^2} \\ &= \frac{1}{r^2}\frac{\partial}{\partial r}\left(r^2\frac{\partial}{\partial r}\right) + \frac{1}{r^2}\nabla^2_{\theta,\varphi}. \end{aligned} \tag{3.23}$$

The harmonic trap term is only a function of r due to the isotropy constraint. By the separation of variable, $\psi(r,\theta,\varphi)$ can be written as

$$\psi(r,\theta,\varphi) = \frac{R(r)}{r}Y(\theta,\varphi). \tag{3.24}$$

Substituting Eq. (3.23) and Eq. (3.24) in Eq. (3.22) and multiplying the resulting equation with $r^3/R(r)Y(\theta,\varphi)$, we obtain

$$\frac{r}{R(r)}\frac{d}{dr}\left[r^2\frac{d}{dr}\left(\frac{R(r)}{r}\right)\right] - r^4 + \frac{1}{Y(\theta,\varphi)}\nabla^2_{\theta,\varphi}Y(\theta,\varphi) = -2Er^2. \tag{3.25}$$

Rearranging Eq. (3.25), yields

$$\underbrace{\frac{r}{R(r)}\frac{d}{dr}\left[r^2\frac{d}{dr}\left(\frac{R(r)}{r}\right)\right] - r^4 + 2Er^2}_{\lambda} + \underbrace{\frac{1}{Y(\theta,\varphi)}\nabla^2_{\theta,\varphi}Y(\theta,\varphi)}_{-\lambda} = 0 \tag{3.26}$$

which can be broken down into two separate pieces. The angular part is

$$\nabla^2_{\theta,\varphi}Y(\theta,\varphi) + \lambda Y(\theta,\varphi) = 0. \tag{3.27}$$

The eigenfunctions of the Laplacian operator, $\nabla^2_{\theta,\varphi}$ in Eq. (3.27) are *the spherical harmonics* shown as $Y_{lm}(\theta,\phi)$ with eigenvalues $-\lambda = -l(l+1)$ [9]. In this thesis, we choose the normalization such that

$$Y_{lm}(\theta,\varphi) = (-1)^m\sqrt{\frac{2l+1}{4\pi}\frac{(l-m)!}{(l+m)!}}P_l^m(\cos\theta)e^{im\varphi}, \tag{3.28}$$

where $P_l^m(\cos\theta)$ are *the associated Legendre polynomials* and are defined for $-l \leq m \leq l$. With the convention of normalization as chosen in Eq. (3.28), the spherical harmonics satisfy the orthogonality property on the unit sphere surface.

$$\int d\Omega Y^*_{lm}(\theta,\varphi)Y_{lm}(\theta,\varphi) = \delta_{ll'}\delta_{mm'}, \tag{3.29}$$

where $d\Omega$ is the solid angle.

The radial part of Eq. (3.26) can be separated by inserting λ determined in the angular part and evaluating the derivatives

$$\frac{d^2R(r)}{dr^2} - r^2R(r) - \frac{l(l+1)}{r^2}R(r) + 2E\ R(r) = 0. \tag{3.30}$$

Next, we investigate the boundary consitions. The radial wavefunction should vanish as $r \to \infty$. In this limit, Eq. (3.30) reduces to the following equation.

$$\frac{d^2R(r)}{dr^2} - r^2R(r) = 0. \tag{3.31}$$

whose solution gives the long range behavior of $R(r)$ as $r \to \infty$.

$$R(r) \sim e^{-r^2/2} \tag{3.32}$$

For $r \to 0$, the isotropic harmonic potential vanishes. Therefore, Eq. (3.30) reduces to

$$\frac{d^2R(r)}{dr^2} - \frac{l(l+1)}{r^2}R(r) = 0. \tag{3.33}$$

Eq. (3.33) can be solved by inducing $R(r) \sim r^s$ and solving the characteristic equation for s. This yields

$$R(r) \sim r^{l+1}. \tag{3.34}$$

Combining these limiting cases, the general form of $R(r)$ can be expected to have a general form

$$R(r) \sim r^{l+1}e^{-r^2/2}L(r), \tag{3.35}$$

where $L(r)$ is a function to be determined.

Inserting Eq. (3.35) into Eq. (3.30) and introducing $\rho = r^2$.

$$\rho\frac{d^2L(\rho)}{d\rho^2} + \left(l + \frac{3}{2} - \rho\right)\frac{dL(\rho)}{d\rho} + \left(\frac{E}{2} - \frac{l}{2} - \frac{3}{4}\right)L(\rho) = 0 \tag{3.36}$$

Replacing $l = \alpha - 1/2$ and $(E - l - 3/2)/2 = k$, one obtains

$$\rho\frac{d^2L(\rho)}{d\rho^2} + (\alpha + 1 - \rho)\frac{dL(\rho)}{d\rho} + kL(\rho) = 0. \tag{3.37}$$

Eq. (3.27) is known as *the associated Laguerre equation* and its solutions are *the associated Laguerre polynomials* [31]:

$$L(\rho) = L_k^{\alpha}(\rho) = L_k^{l+1/2}(r^2), \tag{3.38}$$

The associated Laguerre polynomials are expressed in terms of *the confluent hypergeometric functions*:

$$L_k^{l+1/2}(r^2) = \begin{pmatrix} k + l + 1/2 \\ k \end{pmatrix} F(-k, l + 3/2; r^2), \tag{3.39}$$

where $F(-k, l+3/2; r^2)$ is *the confluent hyper-geometric function of the first kind*.

By defining the associated Legendre polynomials with the prefactor in Eq. (3.39), we introduce the following orthogonality relation:

$$\int_0^\infty d\rho\ \rho^l e^{-\rho} L_k^\alpha(\rho) L_{k'}^\alpha(\rho) = \delta_{kk'}. \tag{3.40}$$

The radial part of $\psi(r, \theta, \varphi)$ can then be expressed without the normalization factor as

$$\frac{R_{kl}(r)}{r} \sim r^l e^{-r^2/2} L_k^{l+1/2}(r^2) \tag{3.41}$$

Finally, the total is:

$$\psi_{klm}(r, \theta, \varphi) = N_{kl} r^l e^{-r^2/2} L_k^{l+1/2}(r^2) Y_{lm}(\theta, \varphi). \tag{3.42}$$

The eigenvalue corresponding to the quantum number, (klm), can be derived by reversing the substitution with $k = (E - l - 3/2)/2$.

$$E_{kl} = 2k + l + \frac{3}{2} \tag{3.43}$$

where $2l + 1$ degeneracy can be easily observed due to $-l < m < l$.

The normalization constant, N_{kl}, can be calculated by using the orthonogality property of $\psi_{klm}(r, \theta, \varphi)$.

$$\begin{aligned}
&\int_0^\infty dr \int d\Omega \psi_{klm}(r, \theta, \varphi) \psi_{k'l'm'}(r, \theta, \varphi) \\
&\quad = N_{kl} N_{k'l'} \int_0^\infty r^{l+l'} e^{-r^2} L_k^{l+1/2}(r^2) L_{k'}^{l'+1/2}(r^2) \int d\Omega Y_{lm}(\theta, \varphi) Y_{l'm'}(\theta, \varphi) \\
&\quad = N_{kl} N_{k'l'} \int_0^\infty r^{l+l'} e^{-r^2} L_k^{l+1/2}(r^2) L_{k'}^{l'+1/2}(r^2) \delta_{ll'} \delta_{mm'} \\
&\quad = N_{kl} N_{k'l} \int_0^\infty r^{2l} e^{-r^2} L_k^{l+1/2}(r^2) L_{k'}^{l+1/2}(r^2) = N_{kl} N_{k'l} \delta_{kk'} \\
&\quad = N_{kl}^2 = 1
\end{aligned} \tag{3.44}$$

Thus, no additional normalization constants are required beyond what has already defined. The sum of the kinetic and the trap term of the Hamiltonian is already diagonal in this basis:

$$\langle \psi_{klm} | \hat{H}_{ho} | \psi_{k'l'm'} \rangle = \langle \psi_{klm} | (\hat{T} + \hat{V}_{trap}) | \psi_{k'l'm'} \rangle = (2k + l + 3/2) \delta_{kk'} \delta_{ll'} \delta_{mm'} \tag{3.45}$$

The radial part and the isosurfaces of $\psi_{klm}(r, \theta, \varphi)$ for selected (k, l, m) are displayed in Fig. 3.2 and Fig. 3.3.

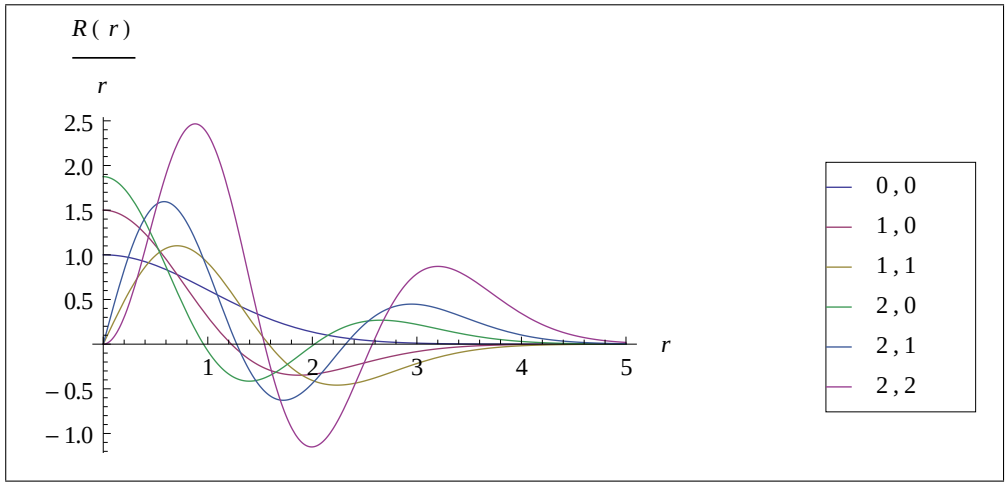

Figure 3.2: The radial part of $\psi_{klm}(r, \theta, \varphi)$ for various (k, l)

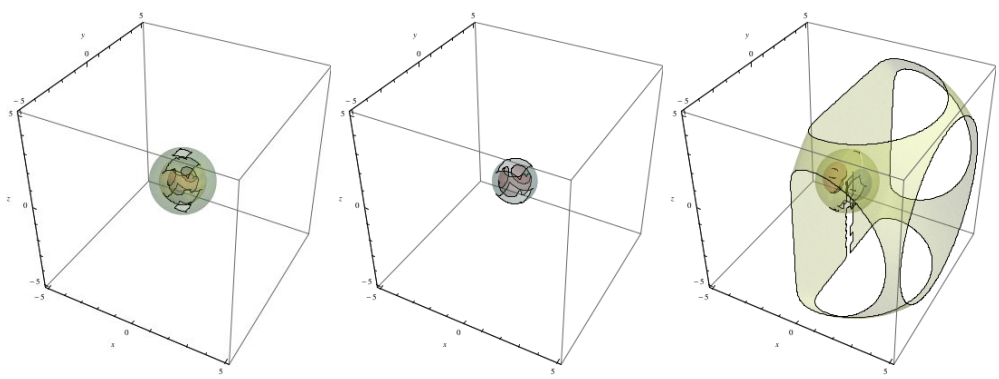

(a) $(k, l, m) = (0, 0, 0)$ (b) $(k, l, m) = (1, 0, 0)$ (c) $(k, l, m) = (1, 1, 1)$

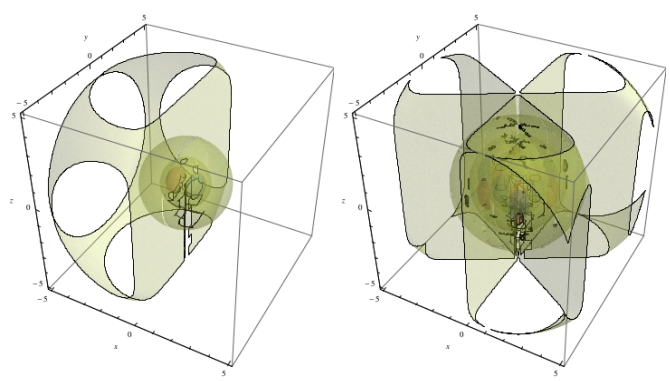

(d) $(k, l, m) = (2, 1, 1)$ (e) $(k, l, m) = (3, 3, 3)$

Figure 3.3: $\psi_{klm}(r, \theta, \varphi)$ for various (k, l, m)

The remaining terms for each element of the Hamiltonian matrix, $\bar{H}$, is written in the

desired basis function set by substituting Eq. (3.42) in (3.20) and using the solution in Eq. (3.45) as

$$\begin{aligned}\langle\psi_{klm}|\hat{H}_{eff}|\psi_{k'l'm'}\rangle &= \langle\psi_{klm}|\hat{T}+\hat{V}_{trap}|\psi_{k'l'm'}\rangle + \langle\psi_{klm}|\hat{V}_{dd}+\hat{V}_{xc}|\psi_{k'l'm'}\rangle \\ &= (2k+l+3/2)\delta_{kk'}\delta_{ll'}\delta_{mm'} + \langle\psi_{klm}|\hat{V}_{dd}+\hat{V}_{xc}|\psi_{k'l'm'}\rangle.\end{aligned} \tag{3.46}$$

The dipole-dipole (Hartree) and the exchange-correlation terms contribute to the off-diagonal entities in $\bar{H}$. The Hartree term is calculated via numerical integration using

$$\langle\psi_{klm}|\hat{V}_{dd}|\psi_{k'l'm'}\rangle = g\int\int d^3r'\ d^3r\ \psi_{k'l'm'}(\vec{r}')\psi_{klm}(\vec{r})\frac{1-3\cos^2\theta_{\vec{r}\vec{r}'}}{|\vec{r}-\vec{r}'|^3}. \tag{3.47}$$

The exchange-correlation potential is to be determined in the next section.

3.4 The Exchange-Correlation Energy

The approximations used in DFT to express the total energy as the functional of the spatial density were discussed in the previous chapter. The required corrections to the Hamiltonian are added in the term V_{xc} under the local density approximation (LDA). The uniform dipolar Fermi gas in the absence of the harmonic trap potential is used to derive LDA corrections in the DFT treatment. The Hamiltonian describing such a uniform gas is

$$\begin{aligned}\hat{H}_g &= \hat{T}+\hat{V}_{dd} \\ &= -\frac{\hbar^2}{2m}\sum_i^N \nabla_i^2 + \frac{1}{2}\frac{\mu_0\mu^2}{4\pi}\sum_i^N\sum_{j\neq i}^N \frac{1-3\cos^2\theta_{ij}}{|\vec{r}_i-\vec{r}_j|^3}.\end{aligned} \tag{3.48}$$

In contrast to the electron gas, there is no *positive background*. The stability of the uniform gas is provided by the angular dependence of the attractive or repulsive characters of the interparticle interactions.

Perturbation theory within second quantization formulation will be applied, the number and the volume of the system can be perturbed simultaneously to keep the density fixed:

$$n_g = \frac{N}{V} \tag{3.49}$$

where n_g is the density of the gas and constant by construction of the gas, while V is the volume of the model system.

The general expression for the second quantized Hamiltonian for the fermionic system can be written in the Dirac notation [16]:

$$\hat{H}_g = \sum_{\vec{k_1},\vec{k_2}} \hat{a}^\dagger_{\vec{k}_1} \langle k_1|\hat{T}|k_2\rangle \hat{a}_{\vec{k}_2} + \frac{1}{2} \sum_{\vec{k_1},\vec{k_2},\vec{k_3},\vec{k_4}} \hat{a}^\dagger_{\vec{k}_1} \hat{a}^\dagger_{\vec{k}_2} \langle k_1 k_2|\hat{V}_{dd}|k_3 k_4\rangle \hat{a}_{\vec{k}_4} \hat{a}_{\vec{k}_3} \tag{3.50}$$

where $\hat{a}^\dagger$ and $\hat{a}$ are the fermionic creation and annihilation operators respectively.

The kinetic energy and the Hartree terms are calculated in the planewave basis with

$$\langle r|k\rangle = \frac{1}{\sqrt{V}} e^{i\vec{k}\cdot\vec{r}}, \tag{3.51}$$

where V is the volume of the sample. Evaluating the kinetic energy term with in the momentum basis .

$$\begin{aligned} \langle k_1|\hat{T}|k_2\rangle &= -\frac{\hbar^2}{2m}\frac{1}{V}\int d^3r e^{-i\vec{k}_1\cdot\vec{r}} \nabla^2 e^{i\vec{k}_2\cdot\vec{r}} \\ &= \frac{\hbar^2 k_2^2}{2m}\frac{1}{V}\int d^3r e^{i(\vec{k}_2-\vec{k}_1)\cdot\vec{r}} = \frac{\hbar^2 k_2^2}{2m}\delta_{k_1 k_2} \end{aligned} \tag{3.52}$$

The Hartree term needs a slightly more challenging treatment:

$$\langle k_1 k_2|\hat{V}_{dd}|k_3 k_4\rangle = \frac{\mu_0 \mu^2}{4\pi}\frac{1}{V^2}\int d^3r\ d^3r\ ' e^{-i\vec{k}_1\cdot\vec{r}} e^{-i\vec{k}_2\cdot\vec{r}'} \frac{1-3\cos^2\theta_{\vec{r}\vec{r}'}}{|\vec{r}-\vec{r}'|^3} e^{i\vec{k}_3\cdot\vec{r}} e^{i\vec{k}_4\cdot\vec{r}'} \tag{3.53}$$

Presenting the dipolar strength as follows to simplify the notation,

$$d^2 = \frac{\mu_0 \mu^2}{4\pi} \tag{3.54}$$

Eq. (3.53) reduces with substitutions $\vec{\rho} = \vec{r} - \vec{r'}$ and $\vec{\rho'} = \vec{r'}$ to

$$\begin{aligned} \langle k_1 k_2|\hat{V}_{dd}|k_3 k_4\rangle &= \frac{d^2}{V^2}\int d^3\rho' e^{-i(\vec{k}_1+\vec{k}_2-\vec{k}_3-\vec{k}_4)\cdot\vec{\rho}'} \int d^3\rho e^{-i(\vec{k}_1-\vec{k}_3)\cdot\vec{\rho}} \frac{1-3\cos^2\theta}{\rho^3} \\ &= \frac{d^2}{V}\delta_{\vec{k}_1+\vec{k}_2,\vec{k}_3+\vec{k}_4} \int d^3\rho e^{-i(\vec{k}_1-\vec{k}_3)\cdot\vec{\rho}} \frac{1-3\cos^2\theta}{\rho^3}. \end{aligned} \tag{3.55}$$

The dipole term becomes from the multipole expansion of $1/\rho$:

$$\frac{1-3\cos^2\theta}{\rho^3} = -\frac{\partial^2}{\partial z^2}\left[\frac{1}{\rho}\right], \tag{3.56}$$

where $\vec{r} = (x, y, z)$.

Using the identity in Eq. (3.57), replacing $(\vec{k}_1 - \vec{k}_3)$ by $\vec{q}$ and applying the rule for the derivative theorem of the Fourier transform [26]:

$$\langle k_1 k_2 | \hat{V}_{dd} | k_3 k_4 \rangle = -\frac{d^2}{V} \delta_{\vec{k}_1+\vec{k}_2,\vec{k}_3+\vec{k}_4} \int d^3\rho e^{-i\vec{q}\cdot\vec{\rho}} \frac{\partial^2}{\partial z^2} \left[\frac{1}{\rho}\right] \tag{3.57}$$

Rewriting Eq. (3.57) in the Cartesian coordinates,

$$\begin{aligned}\langle k_1 k_2 | \hat{V}_{dd} | k_3 k_4 \rangle = -\frac{d^2}{V} \delta_{\vec{k}_1+\vec{k}_2,\vec{k}_3+\vec{k}_4} \int_{-\infty}^{\infty} dx e^{-iq_x x} \int_{-\infty}^{\infty} dy e^{-iq_y y} \\ \times \int_{-\infty}^{\infty} dz\ e^{-iq_z z} \frac{\partial^2}{\partial z^2} \left[\frac{1}{\rho}\right]\end{aligned} \tag{3.58}$$

Applying the derivative theorem again and rewriting in a compact form,

$$\begin{aligned}\langle k_1 k_2 | \hat{V}_{dd} | k_3 k_4 \rangle &= -\frac{d^2}{V} \delta_{\vec{k}_1+\vec{k}_2,\vec{k}_3+\vec{k}_4} (-iq_z)^2 \int d^3\rho e^{-i\vec{q}\cdot\vec{\rho}} \frac{1}{\rho} \\ &= -\frac{4\pi d^2}{V} \delta_{\vec{k}_1+\vec{k}_2,\vec{k}_3+\vec{k}_4} \frac{q_z^2}{q^2}\end{aligned} \tag{3.59}$$

The second quantized many-body Hamiltonian in Eq. (3.50) is expressed explicitly by substituting $\vec{k}_1 = \vec{k} + \vec{p}$, $\vec{k}_2 = \vec{p} - \vec{q}$, $\vec{k}_3 = \vec{k}$ and $\vec{k}_4 = \vec{p}$. The final form of the gas Hamiltonian is

$$\hat{H}_g = \sum_{\vec{k}} \frac{\hbar^2 k^2}{2m} \hat{a}^\dagger_{\vec{k}} \hat{a}_{\vec{k}} - \frac{1}{2} \frac{4\pi d^2}{V} \sum_{\vec{k}\vec{p}\vec{q}} \frac{q_z^2}{q^2} \hat{a}^\dagger_{\vec{k}+\vec{q}} \hat{a}^\dagger_{\vec{p}-\vec{q}} \hat{a}_{\vec{p}} \hat{a}_{\vec{k}} \tag{3.60}$$

where $\hat{a}^\dagger$ and $\hat{a}$ are the creation and annihilation operators respectively.

The perturbing term in the uniform gas Hamiltonian can be revealed by rescaling the uniform gas Hamiltonian with the interparticle distance and the dipole-dipole interaction strength, where it can be defined as

$$V = \frac{4\pi}{3} r_0^3 N \tag{3.61}$$

where V is the total volume,N is the particle number and r_0 is the interparticle distance. The length scale can be defined in analogy to the Bohr radius for the magnetic dipole as

$$a_0 = \frac{m\ d^2}{\hbar^2}. \tag{3.62}$$

where a_0 measures the strength of the dipole-dipole interaction. By the length scale in Eq. (3.62), the dimensionless variable is defined as follows:

$$r = \frac{r_0}{a_0}, \tag{3.63}$$

where large r implies a weak dipole-dipole interaction and diluteness. Rescaling the uniform gas Hamiltonian with the length scale, r_0 leads to $\vec{k} \to \vec{k}/r_0$, $\vec{q} \to \vec{q}/r_0$ and substituting Eq. (3.61) and Eq. (3.63)

$$\hat{H}_g = \frac{d^2}{a_0 r^2} \sum_{\vec{k}} k^2 \hat{a}^\dagger_{\vec{k}} \hat{a}_{\vec{k}} - \frac{1}{2} \frac{3a_0^3 d^2}{2Nr^3} \sum_{\vec{k}\vec{p}\vec{q}} \frac{q_z^2}{q^2} \hat{a}^\dagger_{\vec{k}+\vec{q}} \hat{a}^\dagger_{\vec{p}-\vec{q}} \hat{a}_{\vec{p}} \hat{a}_{\vec{k}} \tag{3.64}$$

Our original system is a dilute Fermi gas and for $r \gg 1$the dominating part is $\hat{H}_0$, since the interaction terms behaves as $1/r$ compared $\hat{H}_0$. Hence $\hat{H}_1$ is chosen the perturbative part of the system.

$$\begin{aligned} \hat{H}_0 &= \frac{d^2}{a_0 r^2} \sum_{\vec{k}} k^2 \hat{a}^\dagger_{\vec{k}} \hat{a}_{\vec{k}} \\ \hat{H}_1 &= -\frac{1}{2} \frac{3a_0^3 d^2}{2Nr^3} \sum_{\vec{k}\vec{p}\vec{q}} \frac{q_z^2}{q^2} \hat{a}^\dagger_{\vec{k}+\vec{q}} \hat{a}^\dagger_{\vec{p}-\vec{q}} \hat{a}_{\vec{p}} \hat{a}_{\vec{k}} \end{aligned} \tag{3.65}$$

The ground state energy of the non-interacting system is equal to the expectation value of $\hat{H}_0$ in the ground state $|F\rangle$ in the occupation number basis representation. $|F\rangle$ preserves the information about the number of particle occupying the possible states.

$$|F\rangle = |n_1 n_2 ... n_\infty\rangle, \tag{3.66}$$

where n_i is the number of particle occupying the ith state and the corresponding energies obey the ascending order, $E_1 < E_2 < ... < E_\infty$. In the fermionic case, n_i is 0 or 1 due to the Pauli exclusion principle. For N particles, then, the ground state is

$$|F\rangle = |\underbrace{111...111}_{N} 0000...\rangle \tag{3.67}$$

where the energy and the momentum of Nth state are defined as *the Fermi energy*, E_F and the *Fermi momentum*, p_F, respectively. The wave number associated with the Fermi momentum is $k_F = p_F/\hbar$. Since two fermions cannot occupy the same state, each fermion can be defined through its wavenumber, $\vec{k}$. Meanwhile, N can be defined through the number operator, $\hat{n}_k$;

$$\begin{aligned} N &= \sum_{\vec{k}} \langle F|\hat{n}_{\vec{k}}|F\rangle = \sum_{\vec{k}} \Theta(k_F - k) = \frac{V}{(2\pi)^3} \int d^3k \Theta(k_F - k) \\ &= \frac{V}{(2\pi)^3} \int d\Omega \int_0^{k_F} dk\ k^2 = \frac{V}{6\pi^2} k_F^3 \end{aligned} \tag{3.68}$$

where Θ is the Heaviside step function.

The zeroth order term is

$$E^0 = \langle F|\hat{H}_0|F\rangle = V\frac{d^2 a_o}{5\pi^2}k_F^5 = V\frac{1}{5\pi^{1/3}}\left(\frac{9}{4}\right)^{5/3}\frac{d^2 a_0}{r_0^5}. \tag{3.69}$$

The zeroth order term corresponds to the total kinetic energy. Then the kinetic energy per volume can be written as

$$\epsilon^0 = \frac{E^0}{V} = \frac{1}{5\pi^{1/3}}\left(\frac{9}{4}\right)^{5/3}\frac{d^2 a_0}{r_0^5}. \tag{3.70}$$

Since the system is perturbed for $1/r \to 0$, the energy per volume can be written as a the power series of $1/r$ assuming that the system is uniform density, $n = N/V$, as:

$$\epsilon = \frac{d^2 a_0}{r_0^5}\left(c_0 + c_1\frac{1}{r} + c_3\frac{1}{r^2}...\right). \tag{3.71}$$

where $c_0 = \frac{1}{5\pi^{1/3}}\left(\frac{9}{4}\right)^{5/3}$ by Eq. (3.70).

Determining the coefficients of the higher order terms in Eq. (3.71) are extremely challenging. However, the second order contribution is relatively feasible.

3.4.1 First Order Correction

The corrections to the ground state of the non-interacting system can be calculated by applying the second quantization perturbation theory to the ground state. The first order correction, $E_{ex}^{(1)}$ is called *the exchange energy*. Fundamentally, the exchange-correlation energy does not have a certain definition. $E^{(1)}$ is called the exchange energy in DFT regarding the equivalent definition in the Hartree-Fock approximation:

$$E^{(1)} = \langle F|\hat{H}_1|F\rangle = -\frac{1}{2}\frac{4\pi d^2}{V}\sum_{\vec{k}\vec{p}\vec{q}}\frac{q_z^2}{q^2}\langle F|\hat{a}^\dagger_{\vec{k}+\vec{q}}\hat{a}^\dagger_{\vec{p}-\vec{q}}\hat{a}_{\vec{p}}\hat{a}_{\vec{k}}|F\rangle \tag{3.72}$$

Considering the properties of the fermionic creation and annihilation operators, $\vec{k}$, $\vec{p}$ and $\vec{q}$ have to satisfy the following conditions:

1. The states represented by $\vec{k}$ and $\vec{p}$ have to be occupied. Otherwise acting on $|F\rangle$ by $\hat{a}$ leads to zero.

2. The states represented by $\vec{k}+\vec{q}$ and $\vec{p}-\vec{q}$ have to be empty.

3. The extracted states by $\hat{a}_{\vec{p}}$ and $\hat{a}_{\vec{k}}$ have to be filled by $\hat{a}^{\dagger}_{\vec{k}+\vec{p}}$ and $\hat{a}^{\dagger}_{\vec{p}-\vec{q}}$.

With these conditions, two different configurations become possible. The first configuration represents *the direct interaction*.

$$\left.\begin{aligned}\vec{k}+\vec{q}=\vec{k}\\ \vec{p}-\vec{q}=\vec{p}\end{aligned}\right\}\Rightarrow \vec{q}=0 \tag{3.73}$$

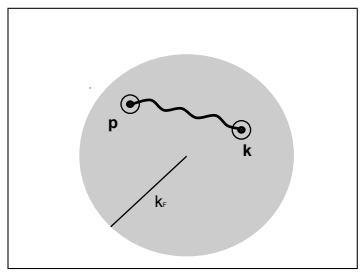

Figure 3.4: The direct interaction in the first order correction

In this case, the destroyed fermions with wavenumbers $\vec{k}$ and $\vec{p}$ are recreated with their previous wavenumbers as illustrated in Fig. 3.4.

$$\begin{aligned}E^{(1)}_{dir} &= -\frac{1}{2}\frac{4\pi d^2}{V}\sum_{\vec{k}\vec{p}}\langle F|\hat{a}^{\dagger}_{\vec{k}}\hat{a}_{\vec{k}}\hat{a}^{\dagger}_{\vec{p}}\hat{a}_{\vec{p}}-\delta_{\vec{k}\vec{p}}a^{\dagger}_{\vec{k}}a_{\vec{k}}|F\rangle\\ &= -\frac{1}{2}\frac{4\pi d^2}{V}\left(\sum_{\vec{k}\vec{p}}\langle F|\hat{a}^{\dagger}_{\vec{k}}\hat{a}_{\vec{k}}\hat{a}^{\dagger}_{\vec{p}}\hat{a}_{\vec{p}}|F\rangle-\sum_{\vec{k}}\langle F|a^{\dagger}_{\vec{k}}a_{\vec{k}}|F\rangle\right)\\ &= -\frac{1}{2}\frac{4\pi d^2}{V}\left(\sum_{\vec{k}\vec{p}}\langle F|\hat{n}_{\vec{k}}\hat{a}_{\vec{p}}|F\rangle-\sum_{\vec{k}}\langle F|\hat{n}_{\vec{k}}|F\rangle\right)\\ &= -\frac{1}{2}\frac{4\pi d^2}{V}\sum_{\vec{k}\vec{p}}\Theta(k_F-k)\Theta(k_F-p)+\frac{1}{2}\frac{4\pi d^2}{V}\sum_{\vec{k}}\Theta(k_F-k)\end{aligned} \tag{3.74}$$

The sums in Eq. (3.74) replaced by integrals, using the appropriate weights, $\frac{V}{(2\pi)^3}$

$$
\begin{aligned}
E^{(1)}_{dir} &= -\frac{1}{2}\frac{4\pi d^2}{V}\frac{V^2}{(2\pi)^6}\int d^3k\ \Theta(k_F-k)\int d^3p\ \Theta(k_F-p) \\
&\quad + \frac{1}{2}\frac{4\pi d^2}{V}\frac{V}{(2\pi)^3}\int d^3k\Theta(k_F-k) \\
&= -\frac{d^2V}{18\pi^3}k_F^6 + \frac{d^2}{9\pi}k_F^3
\end{aligned}
\tag{3.75}
$$

$E^{(1)}_{dir}$ corresponds to the the *direct term* in the HF theory.

The second configuration represents *the exchange interaction* with the conditions

$$
\begin{aligned}
\vec{k}+\vec{q} &= \vec{p} \\
\vec{p}-\vec{q} &= \vec{k}
\end{aligned}
\tag{3.76}
$$

The two destroyed fermions are recreated with a crossover of their wavenumbers, that corresponds to the interaction of two fermions.

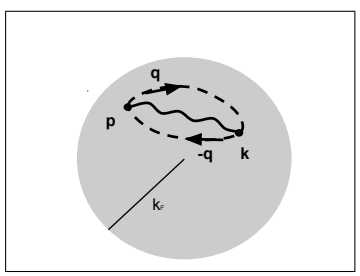

Figure 3.5: The exchange interaction in the first order correction

Eq. (3.72) is rewritten by considering the configuration in Eq. (3.76) representing the exchange interaction as illustrated in Fig. 3.5.

$$
E^{(1)}_{ex} = \langle F|\hat{H}_1|F\rangle = -\frac{1}{2}\frac{4\pi d^2}{V}\sum_{\vec{k}\vec{q}}\frac{q_z^2}{q^2}\langle F|\hat{a}^\dagger_{\vec{k}+\vec{q}}\hat{a}^\dagger_{\vec{k}}\hat{a}_{\vec{k}+\vec{q}}\hat{a}_{\vec{k}}|F\rangle \tag{3.77}
$$

Any swapping between two fermionic operators carries minus sign due to the Fermi statistics. Thus,

$$
\begin{aligned}
E_{ex}^{(1)} &= \frac{1}{2}\frac{4\pi d^2}{V}\sum_{\vec{k}\vec{q}}\frac{q_z^2}{q^2}\langle F|\hat{a}^\dagger_{\vec{k}+\vec{q}}\hat{a}_{\vec{k}+\vec{q}}\hat{a}^\dagger_{\vec{k}}\hat{a}_{\vec{k}}|F\rangle \\
&= \frac{1}{2}\frac{4\pi d^2}{V}\sum_{\vec{k}\vec{q}}\frac{q_z^2}{q^2}\langle F|\hat{n}_{\vec{k}+\vec{q}}\hat{n}_{\vec{k}}|F\rangle \\
&= \frac{2\pi d^2}{V}\sum_{\vec{k}\vec{q}}\frac{q_z^2}{q^2}\Theta(k_F-|\vec{k}+\vec{q}|)\Theta(k_F-k) \qquad (3.78)
\end{aligned}
$$

The summations in Eq. (3.78) can be replaced with the integrals in a similar manner to the direct term

$$
E_{ex}^{(1)} = \frac{1}{2}\frac{Vd^2}{(2\pi)^5}\int\int d^3q\, d^3k\, \frac{q_z^2}{q^2}\Theta(k_F-|\vec{k}+\vec{q}|)\Theta(k_F-k) \qquad (3.79)
$$

Introducing a new variable $\vec{P}=\vec{k}+\vec{q}/2$, Eq. (3.79) becomes

$$
E_{ex}^{(1)} = \frac{Vd^2}{(2\pi)^5}\int d^3q\, \frac{q_z^2}{q^2}\int d^3P\, \Theta(k_F-|\vec{P}+\frac{1}{2}\vec{q}|)\Theta(k_F-|\vec{P}-\frac{1}{2}\vec{q}|) \qquad (3.80)
$$

The integral over $\vec{P}$ can be calculated by considering the geometric construction seen in Fig. 3.6. The intersecting volume of two spheres in Fig. 3.6 for a certain $\vec{q}$, where $0<q<k_F$ can now be calculated geometrically. With this, Eq. (3.80) becomes

$$
\begin{aligned}
&\int d^3P\, \Theta(k_F-|\vec{P}+\frac{1}{2}\vec{q}|)\Theta(k_F-|\vec{P}-\frac{1}{2}\vec{q}|) \\
&\qquad = \frac{4\pi}{3}k_F^3\left(1-\frac{3}{2}\frac{q}{2k_F}+\frac{1}{2}\frac{q^3}{(2k_F)^3}\right)\Theta\left(1-\frac{q}{2k_F}\right) \qquad (3.81)
\end{aligned}
$$

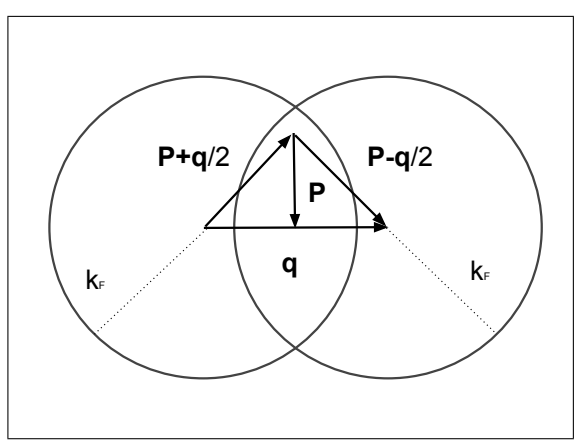

Figure 3.6: The intersecting Fermi spheres

Introducing a new dimensionless variable $\vec{q} = 2k_F\vec{x}$, Eq. (3.81) becomes

$$\begin{aligned} E_{ex}^{(1)} &= -\frac{4Vd^2}{9\pi^3}\int_0^\infty dx\ \left(x^2 - \frac{3x^2}{2} + \frac{x^5}{2}\right)\Theta(1-x) \\ &= -\frac{4Vd^2}{9\pi^3}\int_0^1 dx\ \left(x^2 - \frac{3x^2}{2} + \frac{x^5}{2}\right) \\ &= -\frac{Vd^2}{54\pi^3}k_F^6 \end{aligned} \tag{3.82}$$

$E_{ex}^{(1)}$ is the first order correction to the ground state of the interacting, uniform dipolar Fermi gas and it is equivalent to the *exchange term* in the HF theory. This energy is added as the *exchange energy* to our original system.

Substituting the equality in Eq. (3.68) for k_F

$$E_{ex}^{(1)} = -V\frac{d^2\pi}{3}n^2. \tag{3.83}$$

Then the exchange energy per volume can be written as

$$\epsilon_{ex}^1 = \frac{E_{ex}^{(1)}}{N} = -\frac{d^2\pi}{3}n^2. \tag{3.84}$$

Rescaling n with the harmonic length and rewriting ϵ_{ex}^1 ,n terms of $\hbar\omega$

$$\epsilon_{ex}^1 = -\frac{g\pi}{3}n^2. \tag{3.85}$$

The exchange energy per particle in Eq. (3.85) is used in the computational calculation in this thesis.

The corrections beyond this order are called *the correlation energies*.

3.4.2 Second Order Correction

The second order correction to the ground state is

$$E^{(2)} = \sum_f \frac{\langle F|\hat{H}_1|f\rangle\langle f|\hat{H}_1|F\rangle}{E_0 - E_f} \tag{3.86}$$

where $|f\rangle$ run over states with at most two excitations. The intermediate states represent the case where two fermions in the ground state are excited just above to the Fermi energy, E_F spontaneously and return to the ground states back. There are again two possible process as in the first order correction.

In the direct interaction process, the two fermions are excited by adding a small momentum, $\hbar\vec{q}$ to each with opposite directions to conserve the total momentum and return to their original states as illustrated in Fig. 3.7.

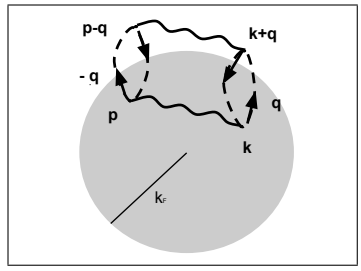

Figure 3.7: The direct interaction in the second order correction

The state $|f\rangle$ represent the possible excitation state of the system with the two hole with the quantum numbers $\vec{k}$ and $\vec{p}$ and the two exited fermions just above k_F with the quantum numbers $\vec{k}+\vec{q}$ and $\vec{p}-\vec{q}$.

$$E^{(2)}_{dir} = \frac{4\pi^2 d^4}{V^2}\frac{\langle F|\hat{H}_1|f\rangle\langle f|\hat{H}_1|F\rangle}{E_0 - E_f} \tag{3.87}$$

The state $|f\rangle$ represents the state, which the two fermions occupy $\vec{k}+\vec{q}$ and $\vec{p}-\vec{q}$.

$$\begin{aligned} E^{(2)}_{dir} = \frac{4\pi^2 d^4}{V^2}\sum_{\vec{q},\vec{k},\vec{p}}\frac{q_z^4}{q^4}\frac{\Theta(|\vec{k}+\vec{q}|-k_F)\Theta(k_F-k)\Theta(|\vec{p}-\vec{q}|-k_F)\Theta(k_F-p)}{E_{\vec{k},\vec{p}}-E_{\vec{k}+\vec{q},\vec{p}-\vec{q}}} \\ -\sum_{\vec{q}\vec{k}}\frac{q_z^4}{q^4}\frac{\Theta(|\vec{k}+\vec{q}|-k_F)\Theta(k_F-k)}{E_{\vec{k}}-E_{\vec{k}+\vec{q}}} \end{aligned} \tag{3.88}$$

where the $E_{\vec{k},\vec{p}} - E_{\vec{k}+\vec{q},\vec{p}-\vec{q}}$ is the energy difference between $|F\rangle$ and $|f\rangle$.

In the exchange interaction, the two excited fermions return back to the ground state by changing their states as illustrated in Fig. 3.8.

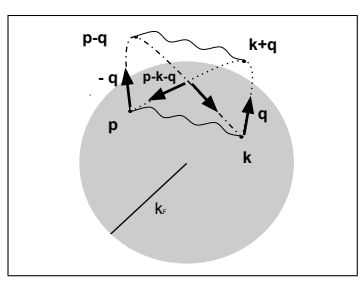

Figure 3.8: The exchange interaction in the second order correction

In the excitation process, the momentum change exchange is with $\vec{q}$, while the momentum exchange is $\vec{p}-\vec{k}-\vec{q}$ in the return to the ground state.

$$\begin{aligned}
\langle f|\hat{H}_1|F\rangle &= -\frac{1}{2}\frac{4\pi d^2}{V}\sum_{\vec{k}\vec{p}\vec{q}}\langle f|\frac{q_z^2}{q^2}\hat{a}^\dagger_{\vec{k}+\vec{q}}\hat{a}^\dagger_{\vec{p}-\vec{q}}\hat{a}_{\vec{p}}\hat{a}_{\vec{k}}|F\rangle \\
&= -\frac{4\pi d^2}{V}\sum_{\vec{k}\vec{p}\vec{q}}\frac{q_z^2}{q^2}\Theta(k_F-k)\Theta(k_F-p) \\
\langle F|\hat{H}_1|f\rangle &= -\frac{1}{2}\frac{4\pi d^2}{V}\sum_{\vec{k}\vec{p}\vec{q}}\langle F|\frac{q_z^2}{q^2}\hat{a}^\dagger_{\vec{k}+\vec{q}}\hat{a}^\dagger_{\vec{p}-\vec{q}}\hat{a}_{\vec{p}}\hat{a}_{\vec{k}}|f\rangle \\
&= -\frac{4\pi d^2}{V}\sum_{\vec{k}\vec{p}\vec{q}}\frac{(\vec{p}-\vec{k}-\vec{q})_z^2}{(\vec{p}-\vec{k}-\vec{q})^2}\Theta(|\vec{k}+\vec{q}|-k_F)\Theta(|\vec{p}-\vec{q}|-k_F) \qquad (3.89)
\end{aligned}$$

Inserting the terms in Eq. (3.89)

$$\begin{aligned}
E_{ex}^{(2)} = \frac{4\pi^2 d^4}{V^2}\sum_{\vec{q},\vec{k},\vec{p}}\frac{q_z^2}{q^2}\frac{(\vec{p}-\vec{k}-\vec{q})_z^2}{(\vec{p}-\vec{k}-\vec{q})^2} \\
\times\frac{\Theta(|\vec{k}+\vec{q}|-k_F)\Theta(k_F-k)\Theta(|\vec{p}-\vec{q}|-k_F)\Theta(k_F-p)}{E_{\vec{k}}-E_{\vec{k}+\vec{q}}}. \qquad (3.90)
\end{aligned}$$

The sums in Eq. (3.89) and Eq. (3.90) are quite challenging. Due to the $1/r^3$ behavior of the dipole term, it is not yet known how the larger order terms behave. Therefore even if the second order corrections may be calculated, higher order terms would have to be also known to understand the full behavior. In this thesis, we limit our correction to only the first order term.

CHAPTER 4

THE NUMERICAL ALGORITHM

The steps of the numerical algorithm are presented implementing a self-consistent solution to the KS equations given Eq. (3.10). The code developed in the C language programming is introduced in pseudo code snippets.

4.0.3 The Predefined Constants

The predefined constants determine the physical system considered and the numerical accuracy of the algorithm.

Algorithm 1 Predefining Global Constants

1: R: The radius of spherical region, where the density is confined.
2: N_r, N_θ, N_φ: The number of points along r, θ, φ respectively
3: K_S:the largest value of the quantum number k of the basis functions
4: R_{cut} : The cut-off interparticle distance in the Hartree term
5: g: The constant in Eq. (3.8)
6: β: The mixing parameter for the previous and new density in iterative procedure
7: N_p: the number of particles

4.0.4 The Generic Functions

The basic functions used during the computational calculation are formed in the preliminary part.

Algorithm 2 The Preliminary Functions

```
function FACTORIAL(Integer)
end function
function DOUBLE FACTORIAL(Integer)
end function
function GAMMA FUNCTION(Integer)
end function
function BASIS FUNCTIONS NUMBER AND QUANTUM NUMBERS(K_S)
    Introduce the total number of the basis functions, N_s
    for 0 ≥ k ≥ K do
        for 0 ≥ l ≥ k do
            for −l ≥ m ≥ l do
                N_S + +
            end for
        end for
    end for
end function
function NORM CONSTANT(Array)
    Calculating the normalization constant of a given array to N_p
end function
function COSINE OF DIFFERENCE VECTOR-DIPOLE ANGLE((r_i, θ_i, φ_i),(r_j, θ_j, φ_j))
    cos θ_ij = |r⃗_i − r⃗_j|_z / |r⃗_i − r⃗_j|
end function
```

The cut-off radius, R_{cut} is also used in Func. 2.20.

4.0.5 The Basis Function Construction

The special functions library of the GNU Scientific Library (GSL) is used to form the basis functions.

Algorithm 3 The Basis Functions

Get $r, \theta, \varphi, k, l, m$
The associated Laguerre polynomial : $L_k^{l+/2}(r^2)$
$L_k^{l+/2}(r^2) = \dfrac{\Gamma(k+l)}{k!\Gamma(l)} gsl_sf_hyperg_1F1(-k, l+1.5, r^2))$
if $m \geq 0$ **then**
    The Spherical Harmonics : $Y_{lm}(\theta, \phi)$
    $Y_{lm}(\theta, \phi) = -1^m * gsl_sf_legendre_sphPlm(l, m, \cos\theta) \cos m\varphi$
else
    if $m < 0$ **then**
        $Y_{lm}(\theta, \phi) = \dfrac{l - |m|}{l + |m|} gsl_sf_legendre_sphPlm(l, m, \cos\theta) \cos m\varphi$
    end if
end if
$\psi_{klm} = e^{-r^2/2} r^l L_k^{l+/2}(r^2) Y_{lm}(\theta, \phi)$

The associated Laguerre polynomials are defined in terms of the confluent hypergeometric function in GSL and the spherical harmonics are constructed by the associated Legendre polynomials produced specially for the spherical harmonic in GSL.

4.0.6 The Hartree Potential

The Hartree potential is formed by using Eq. (3.10). The challenging part is determining the angle between the difference vector, $\vec{r} - \vec{r}'$ and the $z - axis$.

Algorithm 4 The Hartree Potential

Define the difference vector-z axis angle, θ_{ij} by 2.20
procedure HARTREE POTENTIAL($n_n, P(r, \theta, \varphi)$)
    Evaluate the integral in Eq. (3.10)
end procedure

4.0.7 The Hamiltonian Matrix Construction

The Hamiltonian matrix is constructed with the following algorithm.

Algorithm 5 The Hamiltonian Matrix

```
Get r, θ, φ, (k_i, l_i, m_i) ,(k_j, l_j, m_j) and n(r, θ, φ)
Recall N_s from Func. 2.7
for 1 ≤ i ≤ N_s do
    for 1 ≤ j ≤ N_s do
        if i = j then
            H_ij = (2k + l + 3/2) + H^H_ij + H^xc_ij
        else
            H_ij = H^H_ij + H^xc_ij
        end if
    end for
end for
```

4.0.8 The Density Construction

The density is updated by using the KS orbitals and the previous density.

Algorithm 6 Rearranging the Density

```
Assigning n_n to n_p
procedure THE KS ORBITALS(C(klm), P(r, θ, φ))
    Constructing the KS orbitals by Eq. (3.12)
end procedure
Reconstructing n_n by Eq. (3.9)
Normalizing n_n by Func. 2.17
procedure MIXING(n_n, n_p)
    n_n = βn_n + (1 − β)n_p
end procedure
```

where $C(klm)$ is the matrix used to reserve the coefficients in the constructions of the KS orbitals after the solving Eq. (3.18).

4.0.9 The Energy Minimization

The energy is minimized in the iterative process.

Algorithm 7 The Energy Minimization

```
procedure INITIALIZE THE DENSITY(n_n)
    Produce a random density distribution
    Normalize the initial density by Func. 2.17
end procedure
Initializing the energy,E_n
repeat
    procedure THE HAMILTONIAN MATRIX(n_n, P(r, θ, φ), (klm), H)
        Construct the Hamiltonian matrix by 7
    end procedure
    procedure DIAGONALIZATION(H, W)
        Define Lapack variables
        Run Lapack function dsyevd_
    end procedure
    procedure NEW DENSITY(n_n, n_p)
        Using the Alg. 6
    end procedure
    procedure NEW ENERGY(W, E_p, E_n)
        E_p = E_n
        E_n = 0
        for 1 < i < N_p do
            E_n += W[i]
        end for
    end procedure
until E_p < E_n
```

By using this energy minimization scheme, the ground state spatial density is calculated by referring the Hohenberg-Kohn theorems.

CHAPTER 5

RESULTS AND DISCUSSION

In this thesis, we performed numerical calculations to investigate the density profile of the ultracold Fermi gas in a harmonic trap potential. The properties of the system are controlled by two parameters. The first parameter is g in Eq. (3.8), which is determined by the trap frequency, the intrinsic magnetic moment and mass of the atomic species. g controls the density by adjusting the interparticle interactions. The second parameter is the number of the particles, N, which is directly control the density of the system. The behavior of the density profile with respect to these parameters is examined in this section.

5.1 Preliminary Evaluations

Due to the arbitrariness of the choice of R_{cut} and N, we conduct convergence tests with respect to these parameters before the production runs. We expect properties of the such as energy and density profile to be as independent of these parameters as possible provided we choose a good pair.

5.1.1 Choice of R_{cut}

In order to test the effect of R_{cut}, we calculate the Hartree energy of a Gaussian density profile profile for R_{cut} values in range [0,2]. To provide a sense of scale, we note that the radius of our radial mesh is 5 harmonic length.

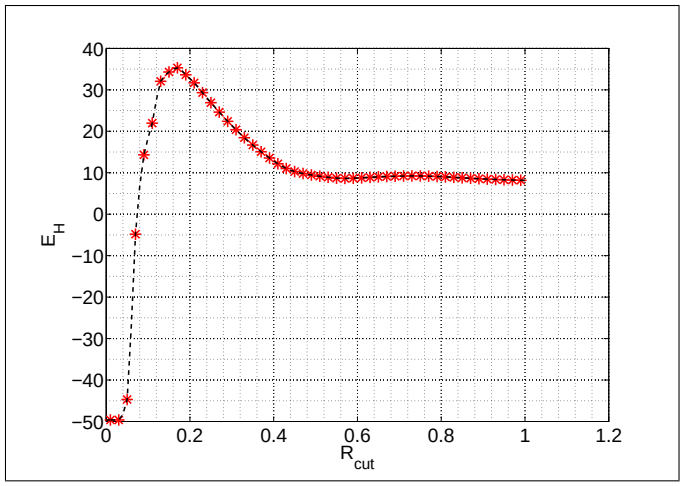

Figure 5.1: The Hartree energy vs. R_{cut} for the Gaussian density distribution

As seen in Fig. 5.1 about $R_{cut} \approx 0.55$ the Hartree energy reaches to a steady region. Therefore, R_{cut} is chosen as 0.55 in the calculations presented in this chapter.

5.1.2 The Number of the Basis Functions

A larger number of the basis functions obviously leads to more accurate numerical results. However, increasing the number of the basis functions in the code increase the running time drastically. Moreover, in order to preserve rotational invariance of the basis set to avoid any angular bias in density profiles, the basis set is expanded via increasing K. Thus, each consecutive K increase N_B by $\sum_{l=0}^{K}(2l+1)$. Therefore, we constraint our calculations to smallest possible K of the basis functions without compromising accuracy.

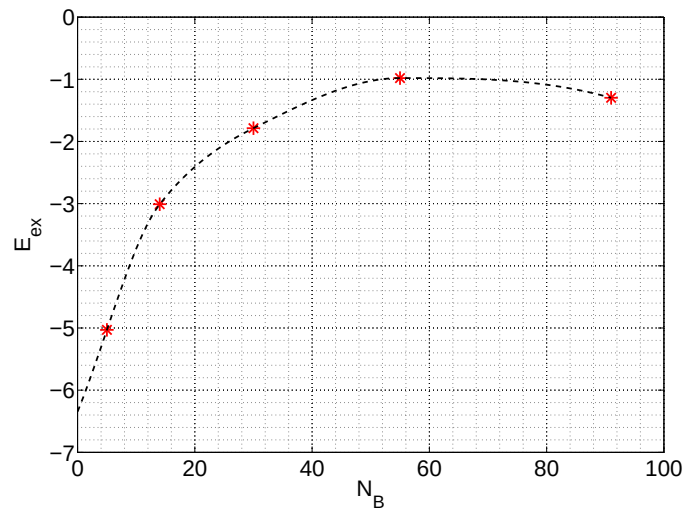

Figure 5.2: The exchange energy at $g = 10.0$ for the various numbers of basis functions, N_B

For $K = 5$, the convergence pattern is somewhat disturbed, possibly due to the fact that the features of the basis functions reduce down to the distance between point in the mesh.

The exchange energy converges asymptotically to -1.0 at $N_B = 55$ as seen in Fig. 5.2. Hence, the number of the basis functions should be chosen at least around $N_B = 55$. In our calculation, N_B was taken as $N_B = 55$, which corresponds to $K = 4$.

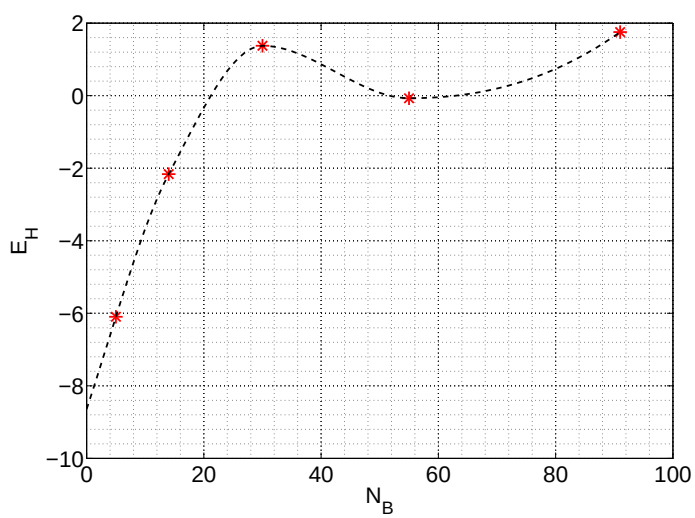

Figure 5.3: The Hartree energy at $g = 10.0$ for the various numbers of basis functions, N_B

The smooth convergence observed in E_{ex} is not observed in E_H as seen in Fig. 5.3. However, a general convergence trend is seen and therefore we assume $N_B = 55$ to be a good enough value.

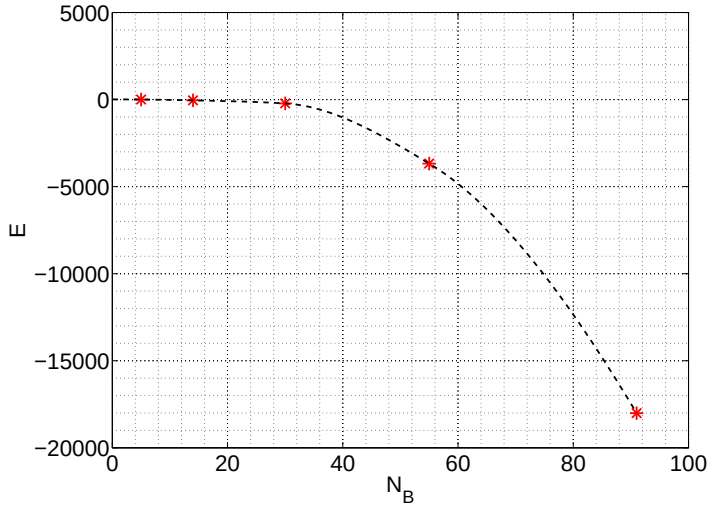

Figure 5.4: The total energy at $g = 10.0$ for the various numbers of basis functions, N_B

5.2 The Density Profile for the Parameter g

The results of the numerical calculations are presented in this subsection for various values of the parameter g. The number of basis function used is $N_B = 55$ corresponding to $K = 4$. The number of points are $N_r = 30$, $N_\theta = 9$ and $N_\varphi = 12$ and the number of particle is taken as $N_P = 4$.

The interaction parameter, g is proportional to the harmonic length, l through the rescaling process, while it is a quadratic function of the intrinsic magnetic moment of the atom species. Larger g represents a tighter confinement by the trap or larger intrinsic magnetic moment. Since the interparticle interaction becomes stronger, the monotonic increase in the exchange energy negatively as seen in Fig. 5.5 is as expected.

The initial oscillating character of the Hartree energy in Fig. 5.6 in the range of the parameter $g \in [1.0, 20.0]$ is in a narrow band. The Hartree energy is highly dependent on the geometry of the final density through the angle dependence of dipoles and g.

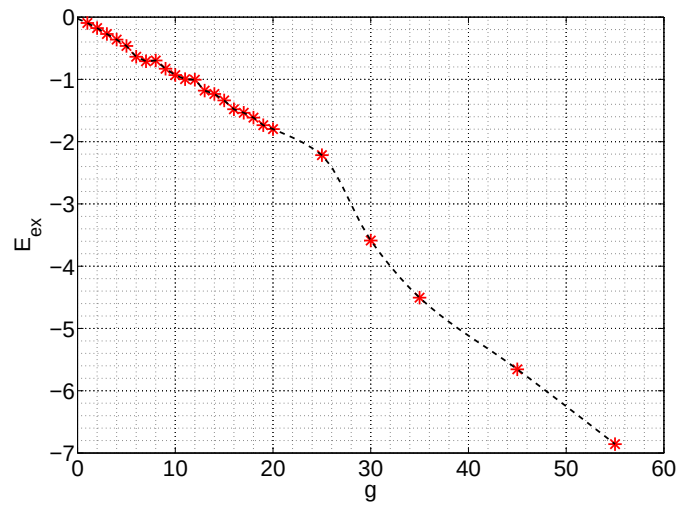

Figure 5.5: The Exchange energy for $K = 4$

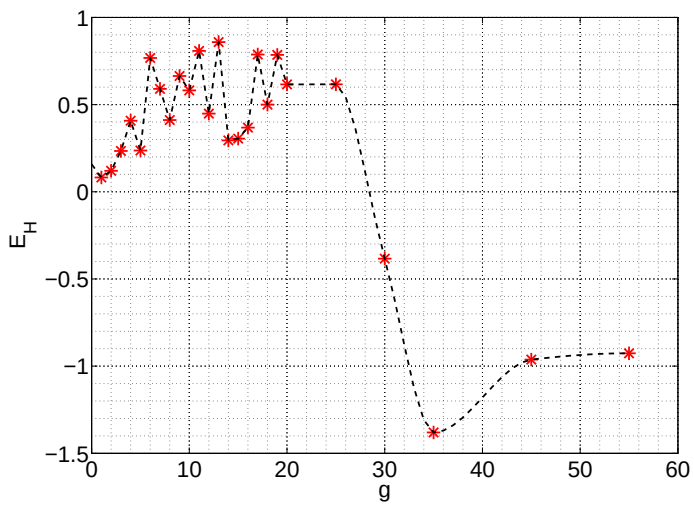

Figure 5.6: The Hartree energy for $K = 4$

Hence, observed oscillations are due to the nature of the Hartree term. This narrow band oscillation character drastically changes for the value of $g > 20$, which implies that the Hartree term becomes less dependent to the geometry and g. This situation will be examined by the density profile for $g = 35.0$ shortly.

What is a more remarkable feature of the system is that the exchange energy is larger than the Hartree energy. This is in contrast with what is generally observed in Coulombic systems, where exchange and correlation are much smaller than the Hartree term.

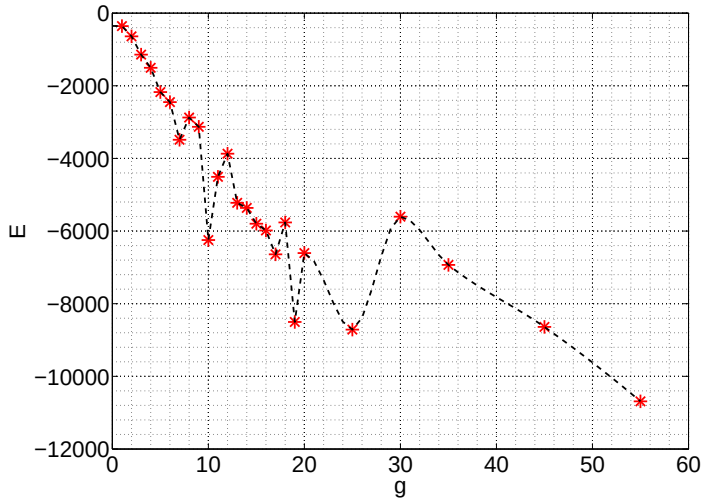

Figure 5.7: The total energy for $K = 4$

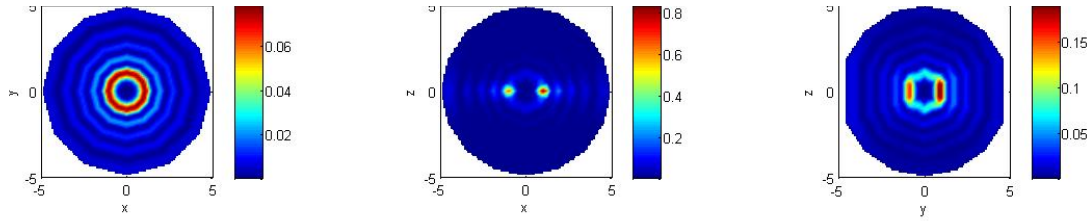

(a) g=1.0

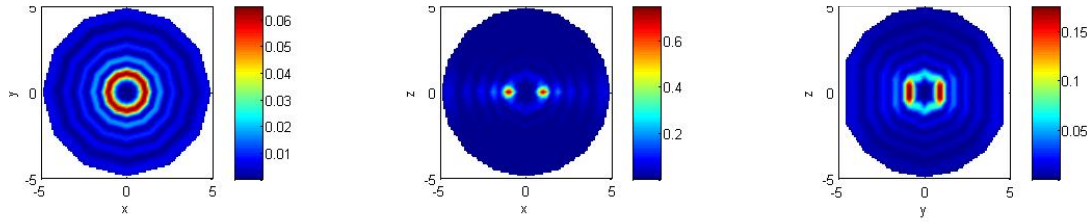

(b) g=2.0

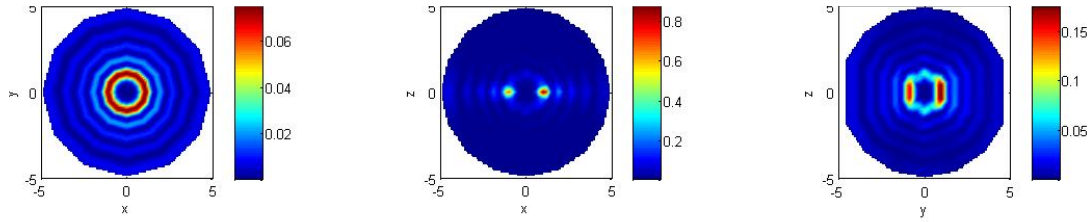

(c) g=3.0

Figure 5.8: The density profiles of planes for $z = 0$, $y = 0$, $x = 0$ respectively for the various g

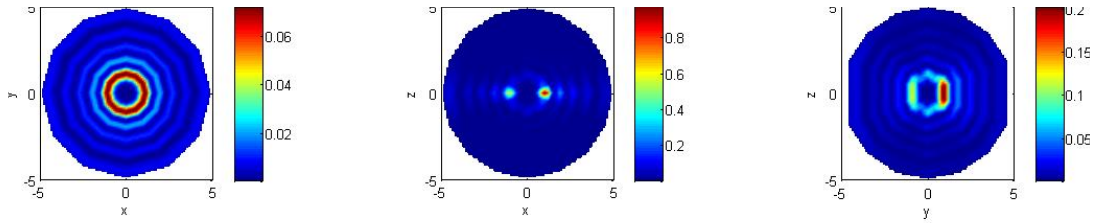

(a) g=4.0

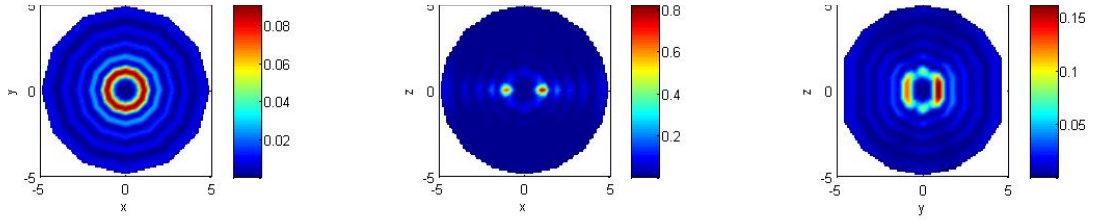

(b) g=5.0

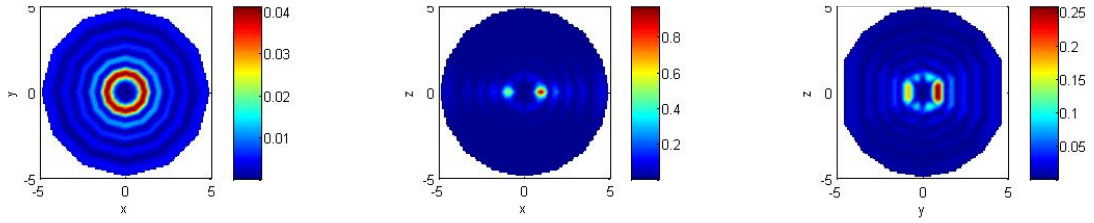

(c) g=6.0

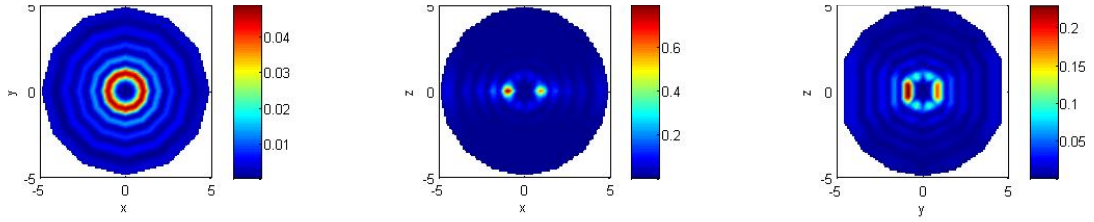

(d) g=7.0

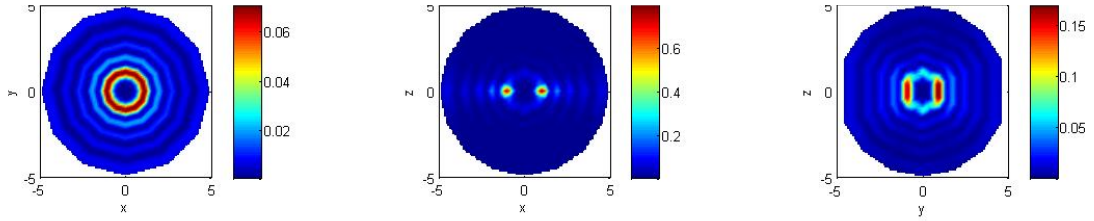

(e) g=8.0

Figure 5.8: The density profiles of planes for $z = 0$, $y = 0$, $x = 0$ respectively for various g (continued)

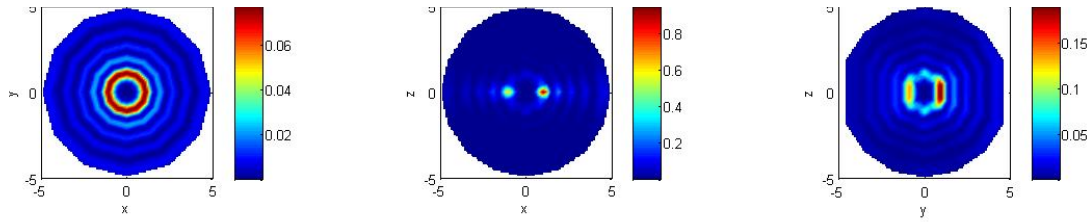

(a) g=9.0

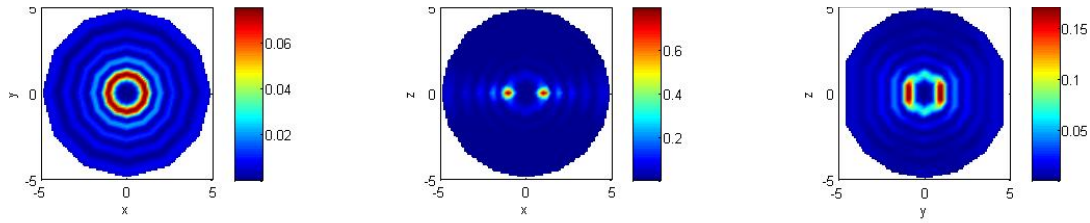

(b) g=10.0

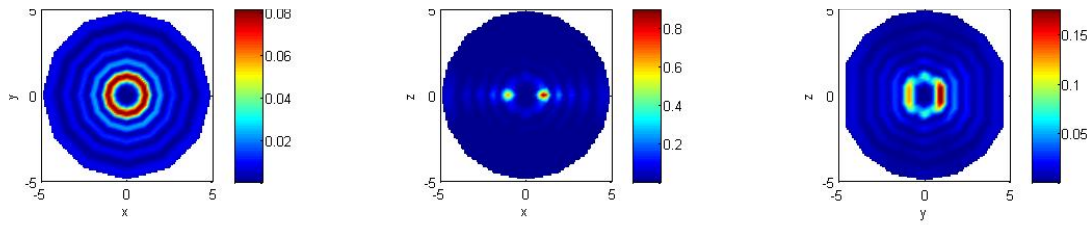

(c) g=11.0

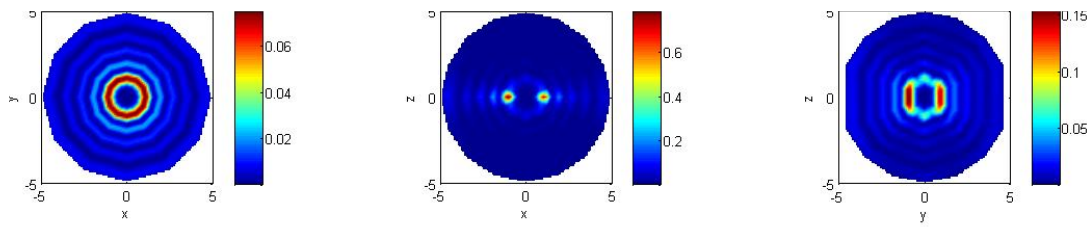

(d) g=12.0

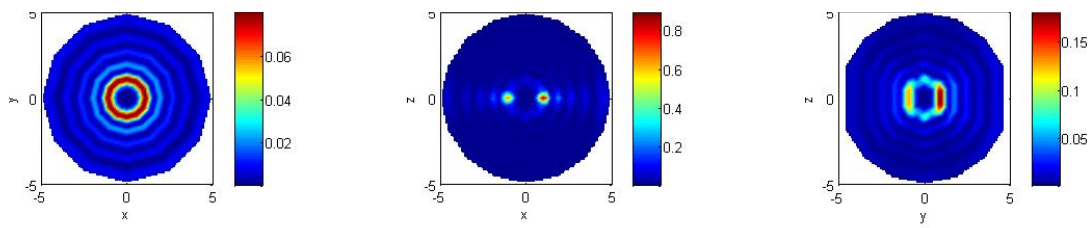

(e) g=13.0

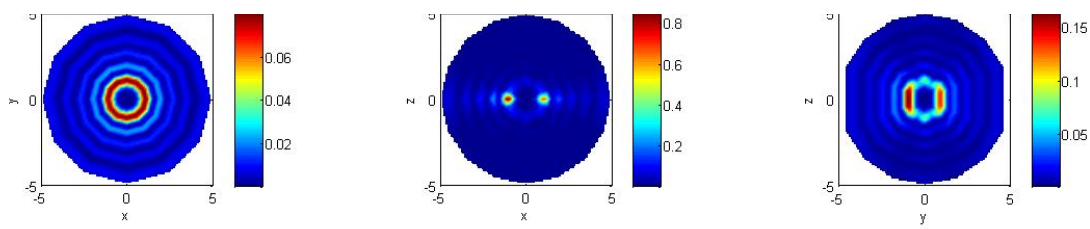

(f) g=14.0

Figure 5.8: The density profiles of planes for $z = 0$, $y = 0$, $x = 0$ respectively for various g (continued)

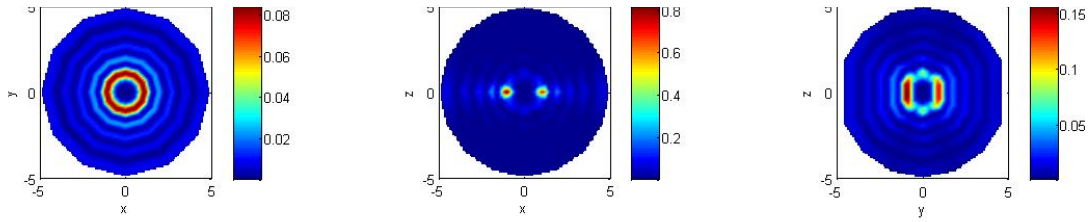

(a) g=15.0

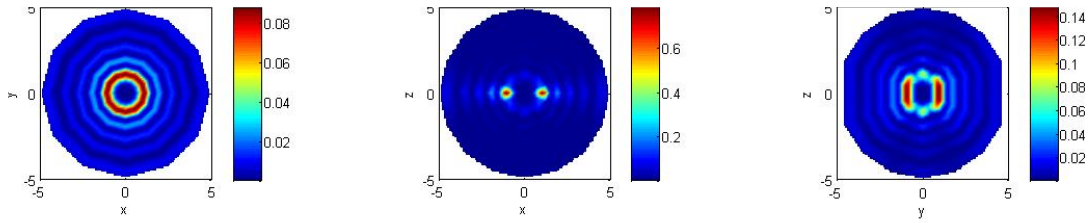

(b) g=16.0

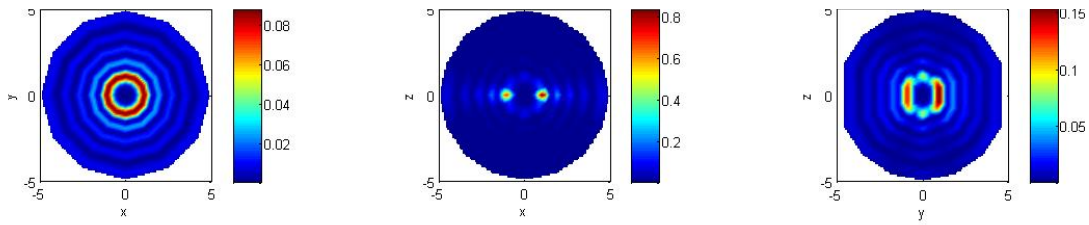

(c) g=17.0

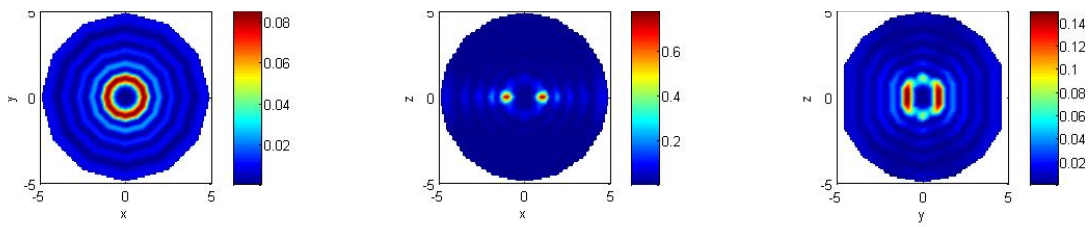

(d) g=18.0

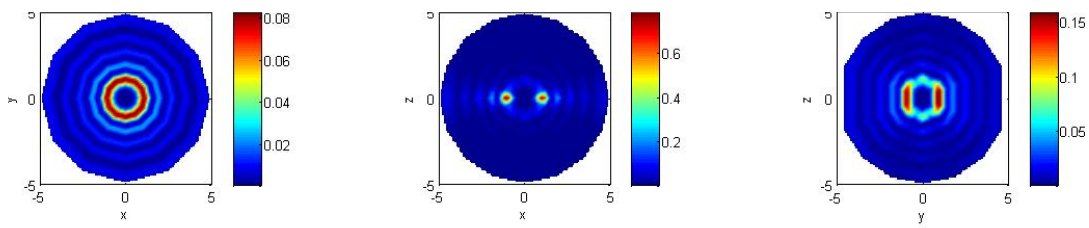

(e) g=19.0

Figure 5.8: The density profiles of planes for $z = 0$, $y = 0$, $x = 0$ respectively for various g (continued)

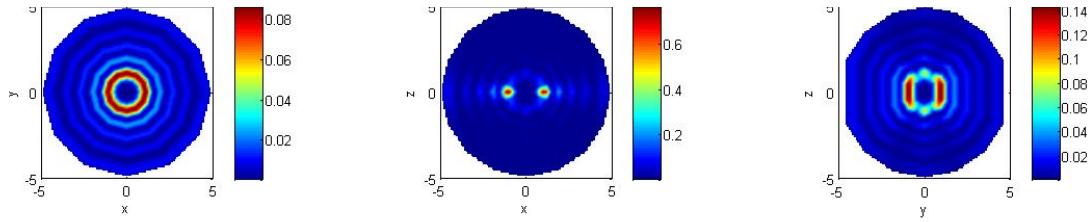

(a) g=20.0

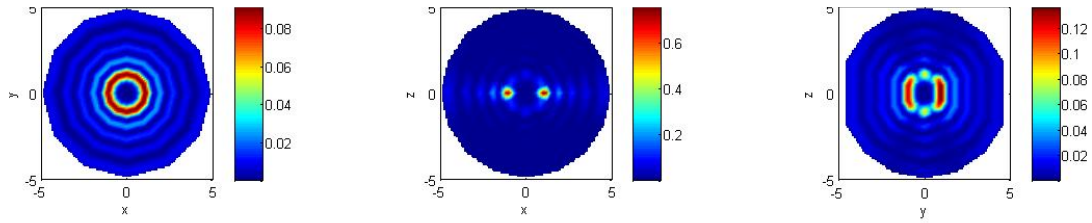

(b) g=25.0

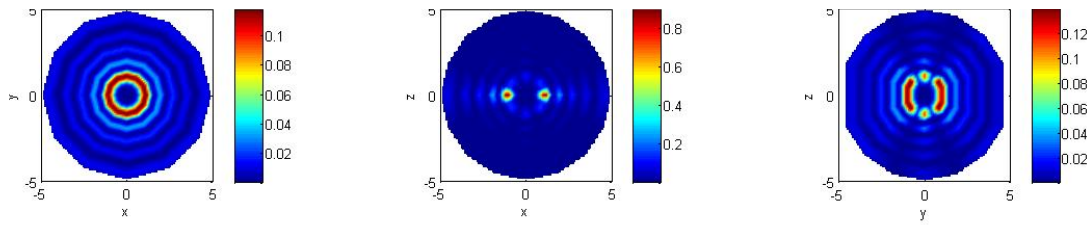

(c) g=30.0

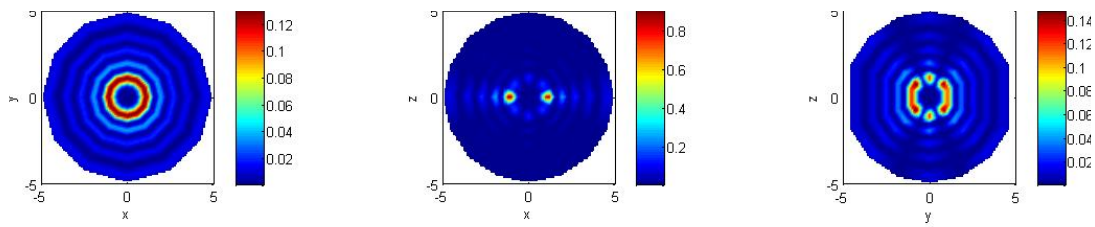

(d) g=35.0

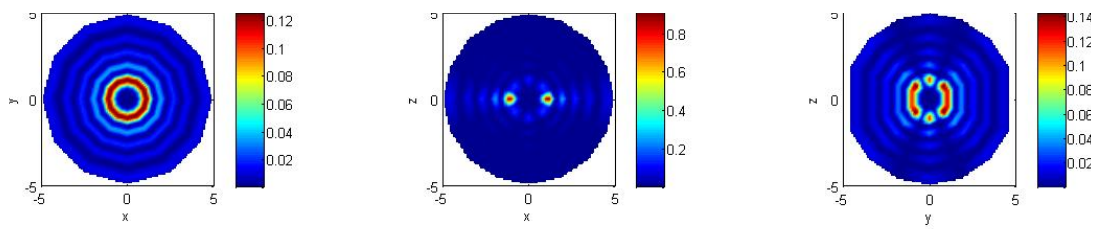

(e) g=45.0

Figure 5.8: The density profiles of planes for $z = 0$, $y = 0$, $x = 0$ respectively for various g (continued)

As clearly seen in Fig. 5.8, the general trend in the density profile is that the particles mostly aggregate along the x-axis with a void centered around the origin. The more detailed density profiles are presented for $g = 7$,$g = 10$, $g = 17$ and $g = 35$ using

contour sketches of chosen planes and the isosurfaces for the various density values. This subgroup is chosen, since each of them have different density profiles and the density profiles for remaining values of g can be grouped under this subgroup.

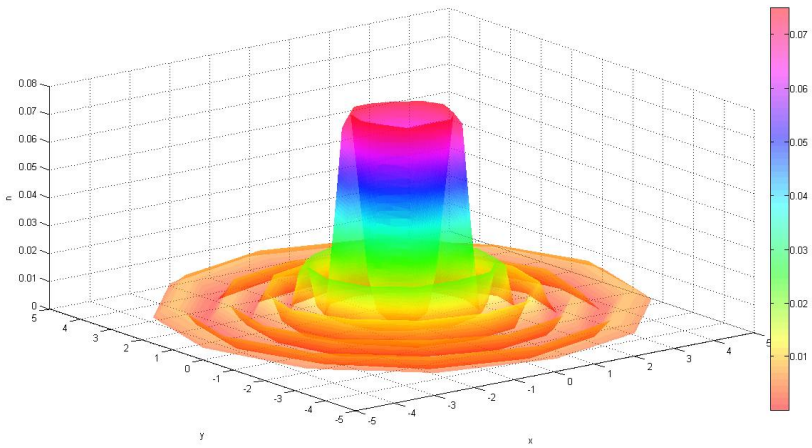

(a) g=10.0,z=0 plane

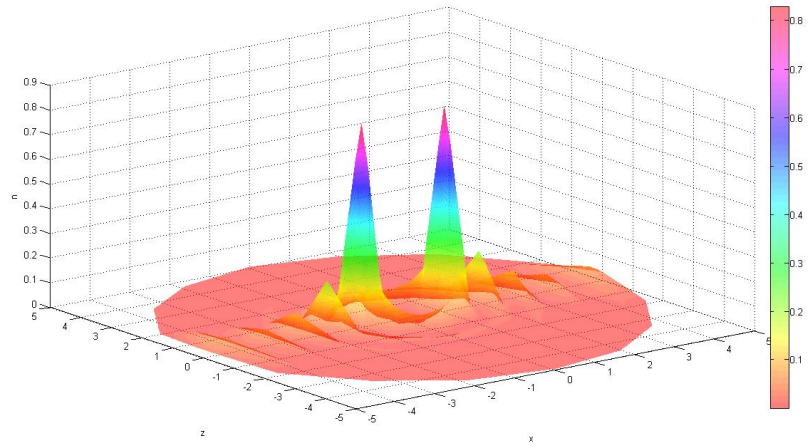

(b) g=10.0,y=0 plane

Figure 5.9: The contour plots of the density profiles of planes for $z = 0$, $y = 0$, $x = 0$ respectively for $g = 10$

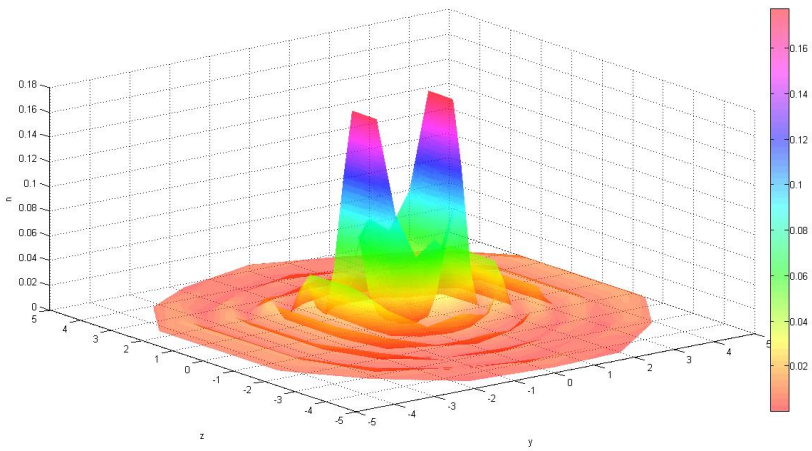

(a) g=10.0,x=0 plane

Figure 5.9: The contour plots of the density profiles of planes for $z = 0$, $y = 0$, $x = 0$ respectively for $g = 10$ (continued)

In Fig. 5.9 (a), the density profile on the xy-plane is the *volcano type*, where there is a crater with the center with the semi-diameter about R_{cut} at the bottom. This volcano type density profile is the signature for every g value. The density in Fig. 5.9 (b) is the *symmetric double well* with sharp peaks, where the density in 5.9 (c) is the *symmetric double well volcano* with blunt peaks and a crater at the center.

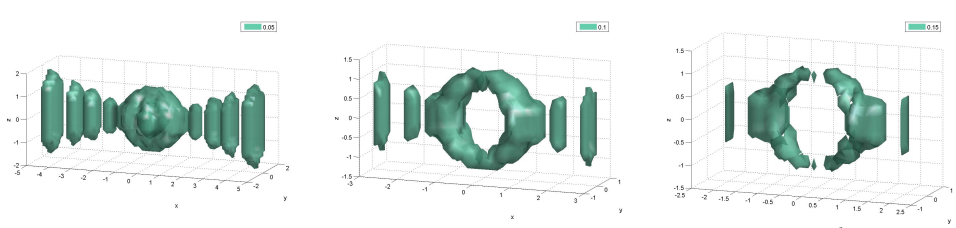

(a) g=10.0,n=0.005 (b) g=10.0,n=0.1 (c) g=10.0,n=0.15

Figure 5.10: The isosurfaces of the various density values for the parameter $g = 10$

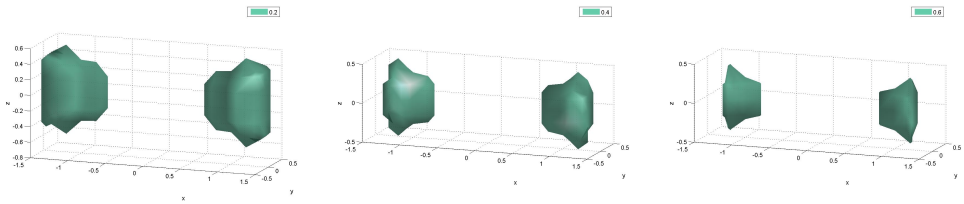

(a) g=10.0,n=0.2 (b) g=10.0,n=0.4 (c) g=10.0,n=0.6

Figure 5.10: The isosurfaces of the various density values for the parameter $g = 10$ (continued)

Some isosurfaces for various density values are represented in Fig. 5.10 at $g = 10.0$. The density has xy-plane, yz-plane and xz-plane mirror symmetries. The particles aggregate around $x \approx 1.0$ and $x \approx -1.0$ densely.

Visualizing the density in the three dimensions is not straightforward. However, considering Fig. Fig. 5.8 and Fig. 5.10, the general geometry can be described as two merged prolate ellipsoids, whose major axises are along x-axis and two condense cores about $x = 1.0$ and $x = -1.0$ as their center. We will refer to them as the *conjoined prolate ellipsoids*. The density profile for g has planer symmetries.

.

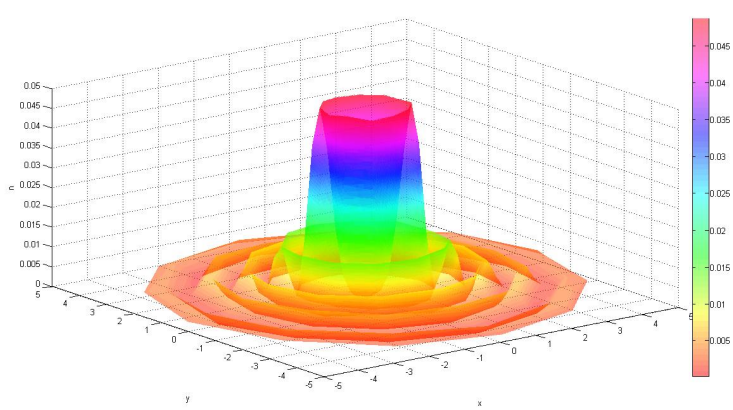

(a) g=7.0,z=0 plane

Figure 5.11: The contour plots of the density profiles of planes for $z = 0$,$y = 0$,$x = 0$ respectively for $g = 7.0$

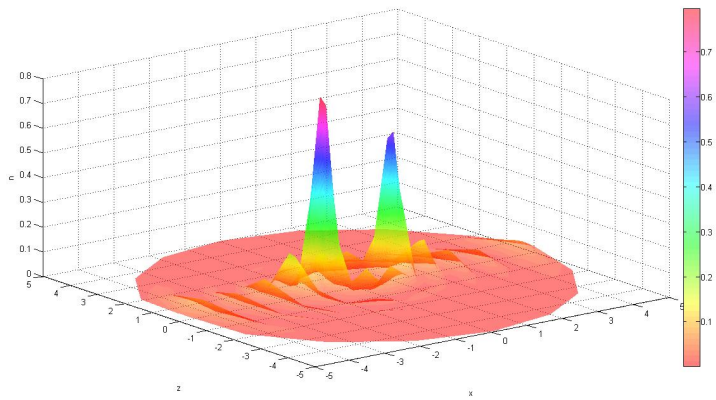

(a) g=7.0,y=0 plane

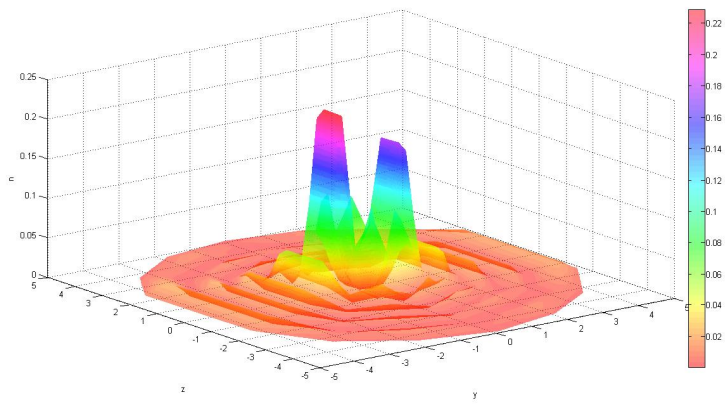

(b) g=7.0,x=0 plane

Figure 5.11: The contour plots of the density profiles of planes for $z = 0$,$y = 0$,$x = 0$ respectively for $g = 7.0$ (continued)

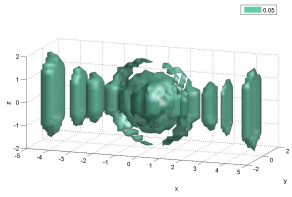

(a) g=7.0,n=0.05

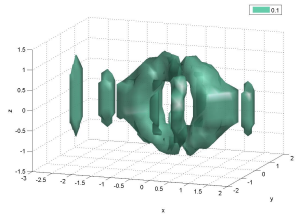

(b) g=7.0,n=0.1

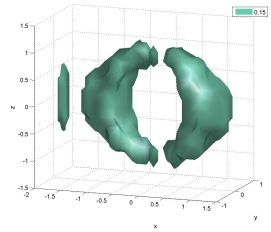

(c) g=7.0,n=0.15

Figure 5.12: The isosurfaces of the various density values for the parameter $g = 7$

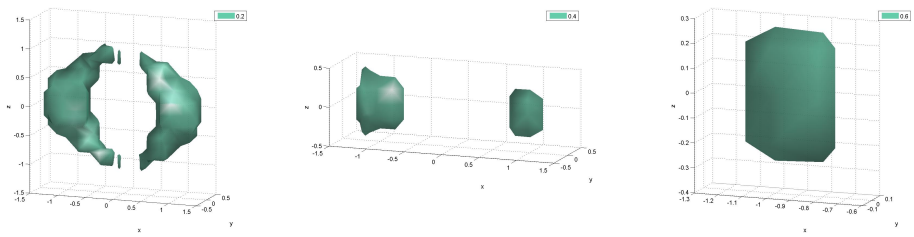

(a) g=7.0,n=0.2 (b) g=7.0,n=0.4 (c) g=7.0,n=0.6

Figure 5.12: The isosurfaces of the various density values for the parameter $g = 7$

The mirror symmetries in xz-plane and yz-plane are broken for $g = 7.0$ as clearly seen in 5.11.

The density concentrates about $x = -1.0$ denser as seen in Fig 5.12. This yields the major axis of the prolate ellipsoid centered about $x = -1.0$ larger than the other centered about $x = 1.0$.

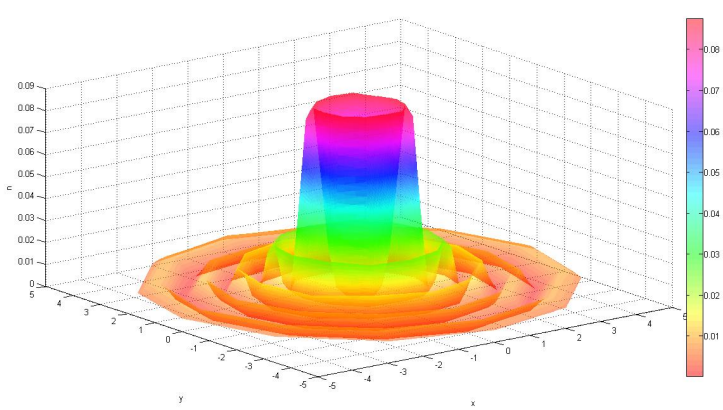

(a) g=17.0,z=0 plane

Figure 5.13: The contour plots of the density profiles of planes for $z = 0$,$y = 0$,$x = 0$ respectively for $g = 17.0$

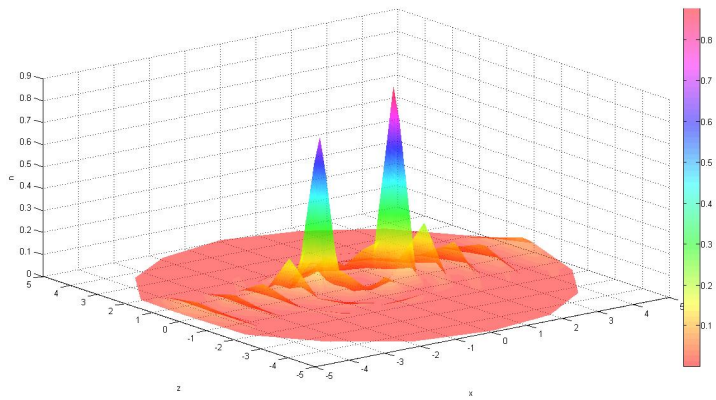

(a) g=17.0,y=0 plane

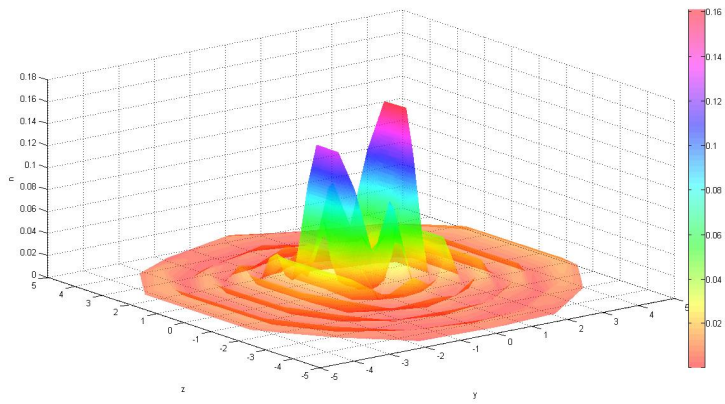

(b) g=17.0,x=0 plane

Figure 5.13: The contour plots of the density profiles of planes for $z = 0$, $y = 0$, $x = 0$ respectively for $g = 17.0$ (continued)

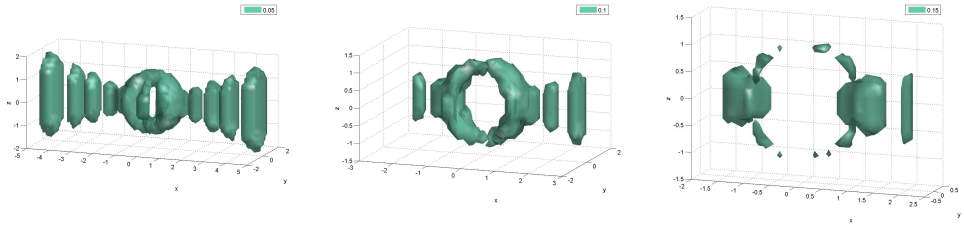

(a) g=17.0,n=0.05 (b) g=17.0,n=0.1 (c) g=17.0,n=0.15

Figure 5.14: The isosurfaces of the various density values for the parameter $g = 17$

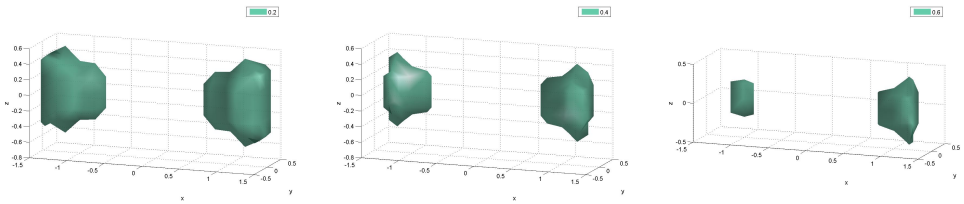

(a) g=17.0,n=0.2 (b) g=17.0,n=0.4 (c) g=17.0,n=0.6

Figure 5.14: The isosurfaces of the various density values for the parameter $g = 17$ (continued)

The mirror symmetries in xz-plane and yz-plane are broken for $g = 17.0$ similarly for $g = 7.0$ as clearly seen in 5.13. Conversely to the situation in $g = 7.0$, the density at the core of the prolate ellipsoid centered at $x = 1.0$ is larger. the density profile for $g = 17.0$ is the mirror symmetric with respect to xz-plane of the density profile for $g = 7.0$.

The asymmetry in the density profiles for $g = 7.0$ and $g = 17.0$ are quite low. This low asymmetry will be clarified in the subsequent section. The remaining density profiles in the range of $g = [1, 20]$ exhibit one of these geometries.

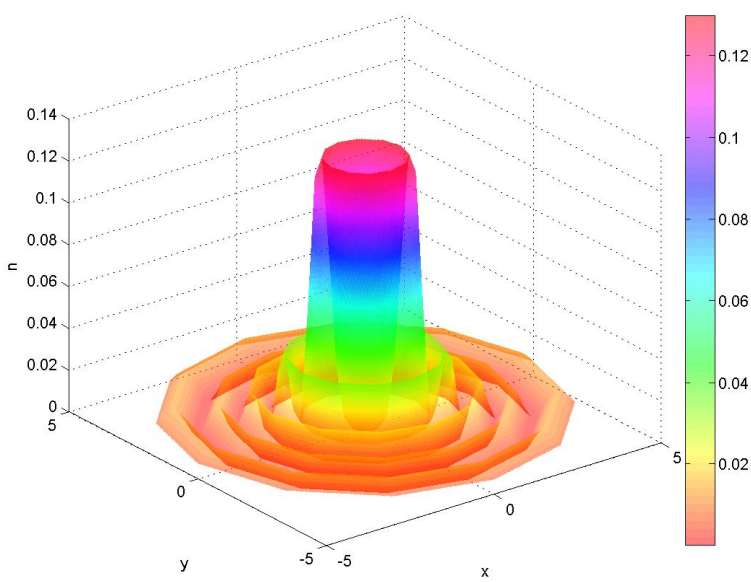

(a) g=35.0,z=0 plane

Figure 5.15: The contour plots of the density profiles of planes for $z = 0$, $y = 0$, $x = 0$ respectively for $g = 35.0$

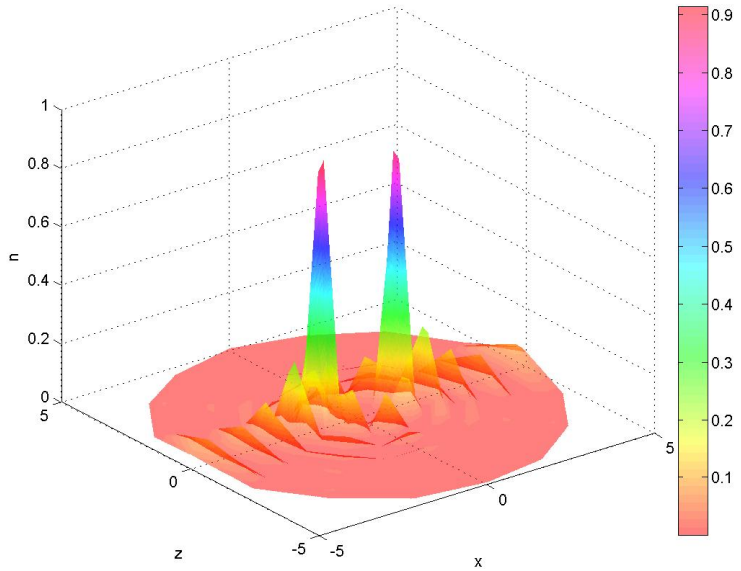

(a) g=35.0,y=0 plane

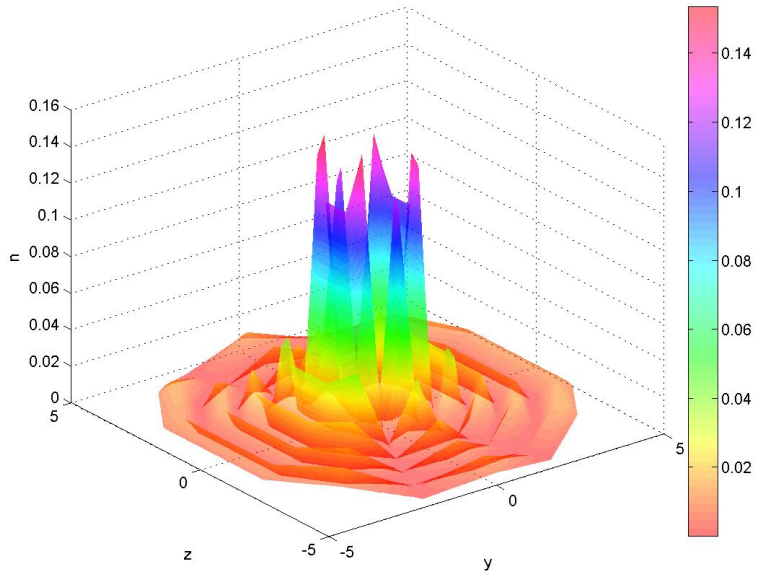

(b) g=35.0,x=0 plane

Figure 5.15: The contour plots of the density profiles of planes for $z = 0$, $y = 0$, $x = 0$ respectively for $g = 35.0$ (continued)

The density profiles for $g > 20$ present different geometries as seen in Fig. 5.8 than the density profiles in range of $1 < g < 20$.

The double well and the double well volcano type density profiles are observed together in the yz-plane as seen in Fig. 5.15. this deformed the conjoined prolate ellipsoid shape.

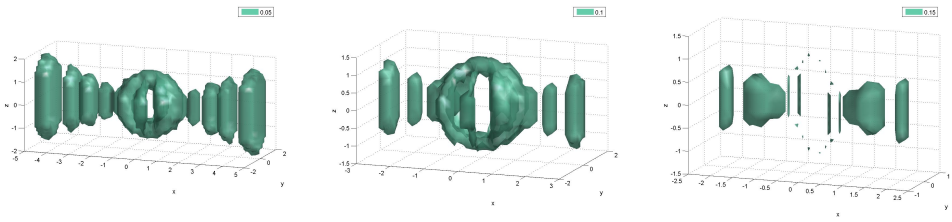

(a) g=35.0,n=0.05 (b) g=35.0,n=0.1 (c) g=35.0,n=0.15

Figure 5.16: The isosurfaces of the various density values for the parameter $g = 35$

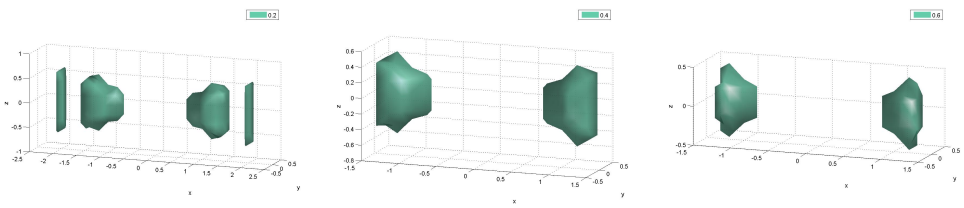

(a) g=35.0,n=0.2 (b) g=35.0,n=0.4 (c) g=35.0,n=0.6

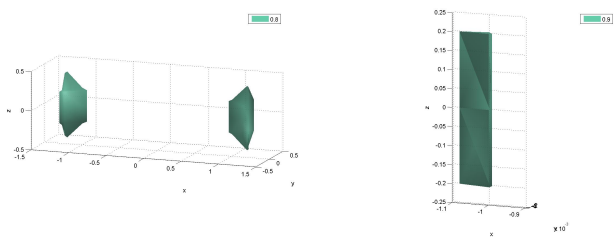

(d) g=35.0,n=0.8 (e) g=35.0,n=0.9

Figure 5.16: The isosurfaces of the various density values for the parameter $g = 35$ (continued)

Examining the isosurfaces in Fig. 5.16, the density disperses along the y-axis and the density profile loses its condensed form is some degree. The transition between the condensed and classical phase is smooth in the Fermi gases. Hence, this smooth change in the density profile is expected.

5.3 The Density Profiles as a function of Number of Particles, N_P

Reminding of the two conditions to observe the Fermi degeneracy discussed in the experimental literature part in the second chapter, one is the sufficient density and the other one is the a sufficient strong harmonic trap.

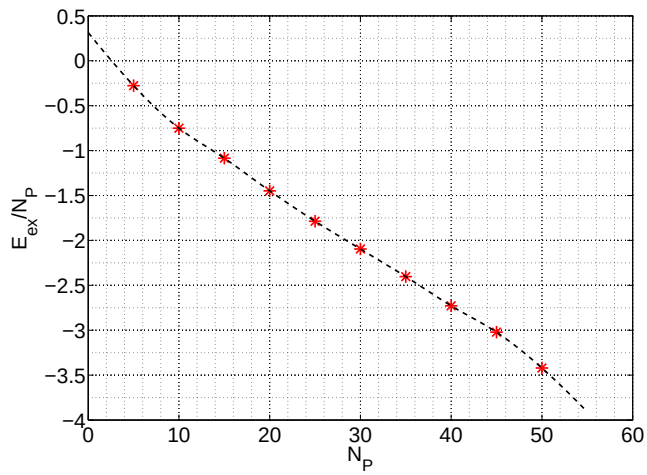

Figure 5.17: The exchange energy at $g = 10$ for the various numbers of particles, N_P

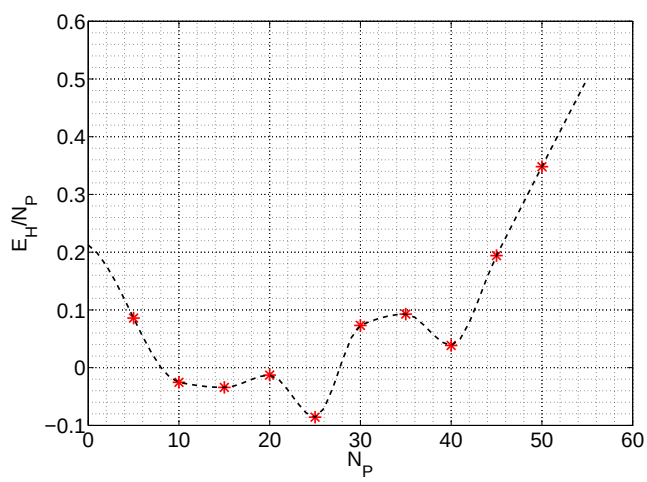

Figure 5.18: The Hartree energy per particle at $g = 10$ for the various numbers of particles, N_P

Increasing the number of particles in the system yields to denser profiles. As a result, the interparticle interactions become larger. Comparing Fig. 5.17 and Fig. 5.18, the exchange energy increases in the negative direction, while the Hartree energy vary in

a quite narrow range for the reasonable range of the particle number. The exchange energy become more prominent in the density profile. This feature of the system is theoretically expected, since the strong correlation nature of the system provides the Fermi degeneracy.

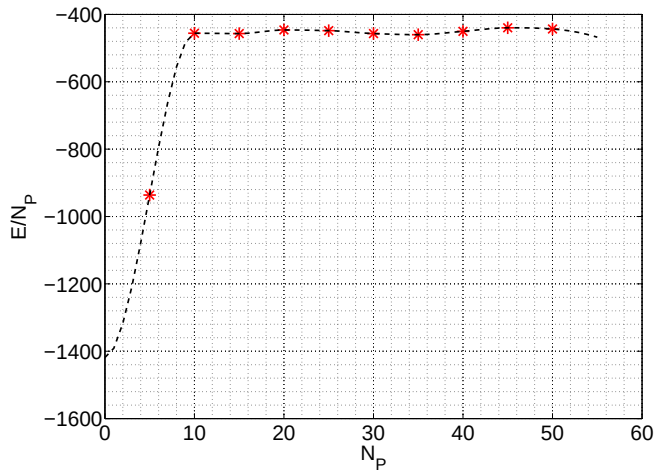

Figure 5.19: The total energy at $g = 10$ for the various numbers of particles, N_P

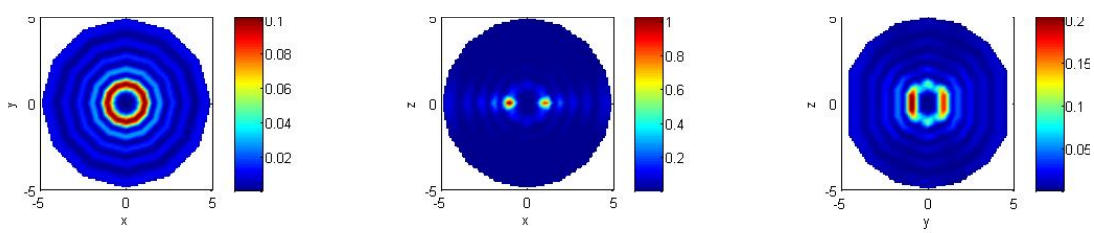

(a) N_B=5

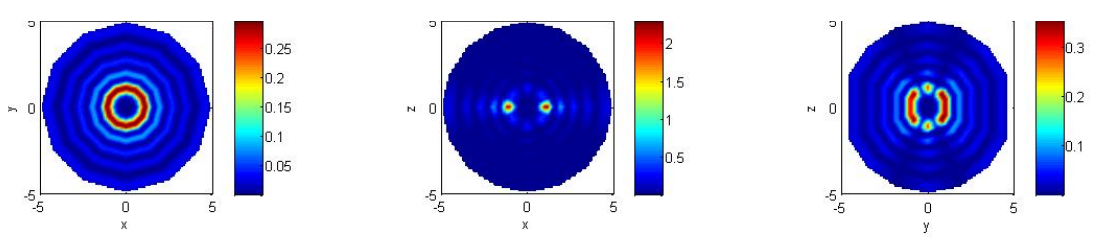

(b) N_B=10

Figure 5.20: The density profiles of planes for $z = 0$,$y = 0$,$x = 0$ respectively at $g = 10$ for various N_B

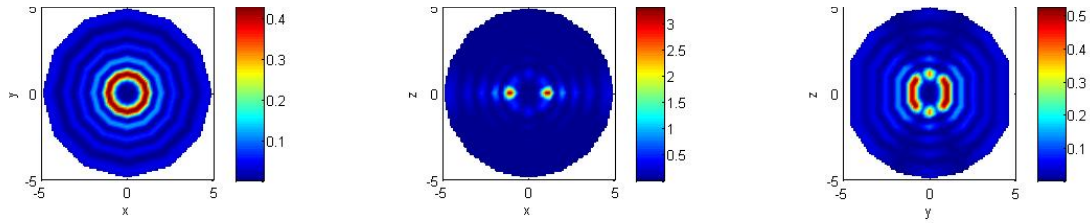

(a) N_B=15

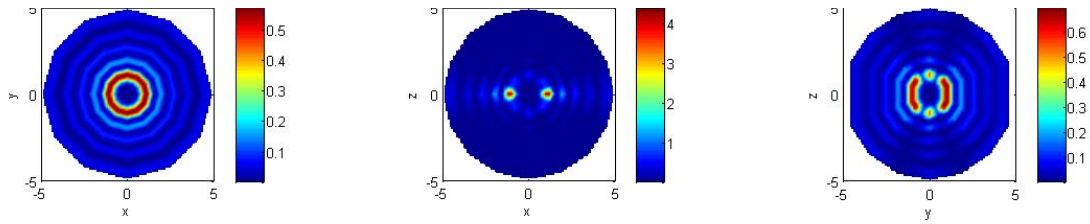

(b) N_B=20

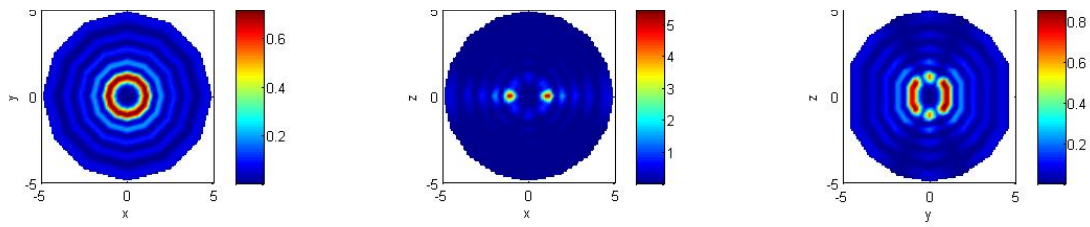

(c) N_B=25

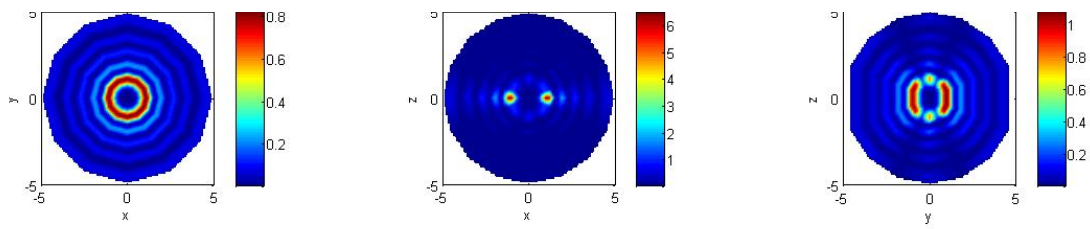

(d) N_B=30

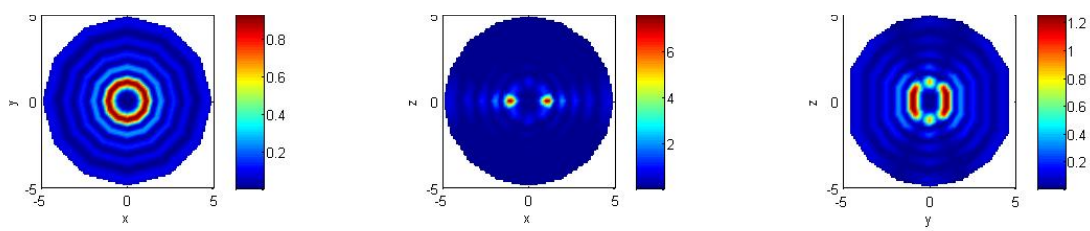

(e) N_B=35

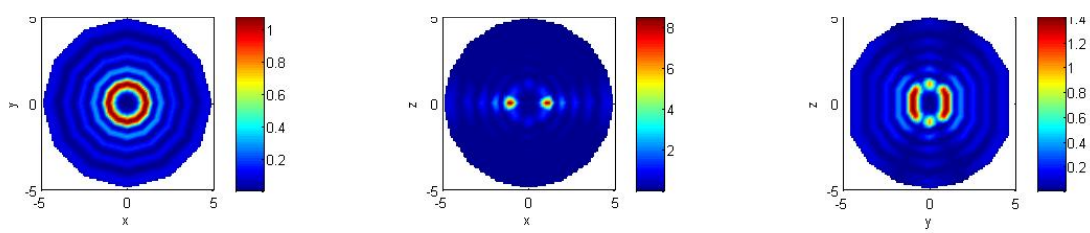

(f) N_B=40

Figure 5.20: The density profiles of planes for $z = 0$,$y = 0$,$x = 0$ respectively at $g = 10$ for various N_B (continued)

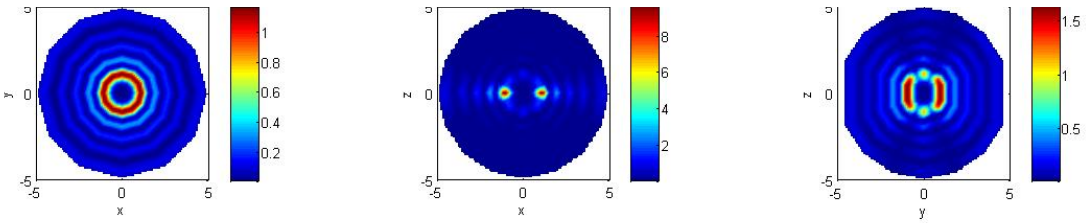

(a) N_B=45

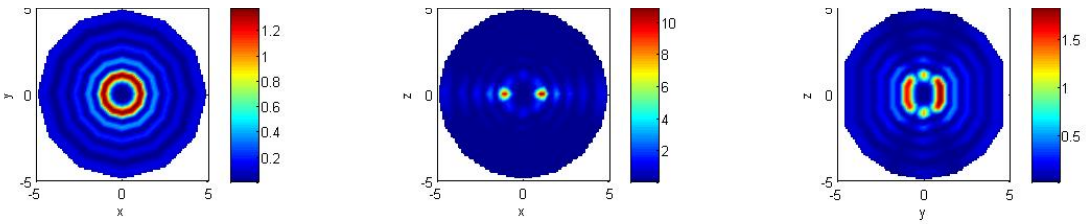

(b) N_B=50

Figure 5.20: The density profiles of planes for $z = 0$,$y = 0$,$x = 0$ respectively at $g = 10$ for various N_B (continued)

Increasing the particle number yields an increase in the overall density as expected. However, examining the density increments along different axises shown in Fig. 5.20 implies that the density aggregates along the x-axis more densely. This asymmetric aggregation stretches the general geometry more along the x-axis with the increasing particle number. This increase the ratio of the major axis and minor axis of the conjoined prolate ellipsoids without changing their centers.

One of the remarkable observations is that the density become symmetric with respect to the xy-plane, yz-plane and xz-plane, where for small particle number, $N_B = 5$, the density is asymmetric. This asymmetric character in the previous part is left as an unanswered question. Hence, it may be claimed that for large particle number, the density profiles become the conjoined prolate ellipsoid for all g. This examination is left for the further studies.

CHAPTER 6

CONCLUSION

In this thesis, an ultracold dipolar Fermi gas under the harmonic traps was investigated using DFT with LDA correction. Experimental studies show that the ultracold Fermi gas in a harmonic trap exhibits quantum mechanical properties and this phenomena called the Fermi degeneracy. Furthermore, the ultracold Fermi gases can condense denser than the Boson gas under the appropriate harmonic trap after the suitable cooling process. Two crucial challenges become significant in the Fermi degeneracy phenomena. The first is cooling the fermions down to the range of nK temperature and the second is to force them to achieve a certain density. The first condition depends on the experimental processes. The second condition is adjusted by the trap parameters and the atomic species used along with a sufficient particle number in the trap geometry. These conditions are implemented in our study through the parameter g and the particle number N_P.

Although the theoretical understanding of the BEC is quite advanced through the ultracold, dilute bosonic gases, the counterpart in the fermionic case is still in progress. There are many approaches and approximations in the literature. In experiments, the Fermi degeneracy cannot be achieved by using a single fermion species. Viable systems are Fermi-Bose mixtures, two fermion species or the single species with different quantum states. As a starting point, however, we are only concerned in this thesis by one component gas.

The relative high density requirement of the Fermi degeneracy leads the system to strongly correlated interparticle interaction. Hence, the exchange-correlation energy becomes significant in the system. The exchange energy to be used in the LDA corre-

lations is calculated using the perturbation theory for a uniform dipolar gas described with the second quantized Hamiltonian. Only the first order correction to the system is included in this study. This contribution to the total energy is called the exchange energy. The contribution of the exchange energy to the total energy of the system is relatively larger than the Hartree energy. Addition to it, the exchange energy becomes larger for larger g values in a reasonable range. Another important observation is that increasing the particle number causes a monotonic increase in the exchange energy, while the Hartree energy varies in a relatively small range.

The density profile of the ultracold Fermi gas is observed as a prolate ellipse in the experimental studies in two dimensional projection [41]. Hence, the expected geometry in three dimensions is proposed to resemble to Gaussian like geometry. The resulting geometry found by the numerical calculations can be described as a conjoined prolate ellipsoid with the major axis along the x-axis, where the density aggregate on the centers of the prolate ellipsoid densely. The separation between the centers of the ellipsoid is about two harmonic length. It is worthy to express that the density profiles are not isotropic, even under the isotropic harmonic trap and aligned dipoles along the z-axis. The non-isotropy of the density is due to the angle dependence of the interparticle interaction.

The integrals are calculated in the code by the trapezoid method. In the debugging process of the code, the oscillating nature of the integrals performed during the numerical calculation depending the number of points chosen is discovered. Since the calculation performed in spherical coordinates, relatively more points can be included around the center, while a smaller number of points can be accounted away from the center.

Further improvement and studies can be done to improve the accuracy of the numerical calculation, decreasing the running time and study more general cases. One such improvement would be to smoothly regularize the $r \approx 0$ region of the interaction rather than introduce a hard cutoff.

The serial code may be parallelize to decrease the running time. This would allow us to perform calculations a larger mesh and particle number. More efficient and accurate methods of integration can be applied to perform the integral in the code.

Finally, more general cases can be investigated by changing the nature of the trap potential. For different geometries, the density profile of the system can be examined. Moreover, the mixture of different atom and molecule species can be considered as well.

REFERENCES

[1] M.H. Anderson, J.R. Ensher, M.R. Matthews, C.E. Wieman, and E.A. Cornell. Observation of Bose-Einstein condensation in a dilute atomic vapor. *Science*, 269:198–201, 1995.

[2] Ashkin Arthur. Trapping of atoms by resonance radiation pressure. *Physical Review Letter*, 40(12), 1978.

[3] T. Bergeman, G. Erez, and H.J. Metcalf. Magnetostatic trapping fields for neutral atoms. *Phys. Rev. A.*, 35(4), 1987.

[4] H.L. Bethlem, G. Berden, F.H.M. Crompvoets, Jongma R.T., A.J.A von Raji, and G. Meijer. Electrostatic trapping of ammonia molecules. *Nature*, 406:491–493, 2000.

[5] N.N. Bogoliubov. On the theory of superfluidity. *Journal of Physics*, 11(1):23–32, 1947.

[6] S.N. Bose. Plancks gesetz und lichtquantenhypothese. *Zeitschrift fur Physik*, 23(178), 1924.

[7] C.C. Bradley, C.A. Sackett, , and R.G. Hulet. Bose-Einstein condensation of lithium:observation of limited condensation number. *Physical Review Letter*, 78(6):985–989, 1997.

[8] D.A. Butts and D.S. Rokhsar. Trapped Fermi gases. *Phys. Rev. A*, 55(6), 1997.

[9] F.W. Byron and R.W. Fuller. *Mathematics of Classical and Quantum Physics*. Dover, New York, 1992.

[10] K.B. Davis, M.O. Mewes, M.R. Andrews, N.J. van Druten, D.S. Durfee, D.M. Kurn, and Ketterle W. Bose-Einstein condensation in a gas of sodium atoms. *Physical Review Letter*, 75(22), 1995.

[11] K.B. Davis, M.O. Mewes, and W. Ketterle. An analytical model for evaporative cooling of atoms. *Appl.Phys.*, B(60):155–159, 1986.

[12] B. DeMarco and D.S. Jin. Onset of Fermi degeneracy in a trapped atomic gas. *Science*, 285:1703–1706, 1999.

[13] P.A.M. Dirac. Note on exchange phenomena in the Thomas atom. *Mathematical Proceedings of the Cambridge Philosophical Society*, 26:376–385, 1930.

[14] A. Einstein. Quantentheorie des einatomigen idealen gases. *Sitzber. Kgl. Preuss. Akad. Wiss.*, 1:3, 1925.

[15] E. Fermi. Un metedo statistico per la determinazione di alcune priopriata dell'atomo. *Rend.Accad.Naz.Lincei*, 6:602–607, 1927.

[16] A.L. Fetter and J.D. Walecka. *Quantum Theory of Many-Particle Systems*. McGraw-Hill, New York, 1971.

[17] S. Giorgini, L.P. Pitaevskii, and S. Stringari. Theory of ultracold atomic Fermi gase. *Rev. Mod. Phys.*, 80(4):1216–1268, 2008.

[18] K. Goral, B.G. Englert, and K. Rzazewski. Semiclassical theory of trapped fermionic dipoles. *Phys. Rev. A*, 63(033606), 2001.

[19] A. Griffim, D.W. Snow, and String S., editors. *Bose-Einstein Condensation*. Cambridge University Press, New York, 1995.

[20] R. Grimm, M. Weidermuller, and Y.B. Ovchinnikov. Optical dipole traps for neutral atoms. *Adv.At.Mol.Phys.*, 42:95–165, 2000.

[21] E.P. Gross. Structure of a quantized vortex in boson systems. *Nuovo Cimento*, 20:454–477, 1961.

[22] T.W. Hansch and A.L. Schawlow. Cooling of gases by laser radiation. *Optics Communication*, 13(1), 1975.

[23] H.F. Hess. Evaporative cooling of magnetically trapped and compressed spin-polarized hydrogen. *Physical Review B*, 34(5), 1986.

[24] K. Hohenberg and W. Kohn. Inhomogeneous electron gas. *Physical Review*, 136(3B), 1964.

[25] M. Inguscio, W. Ketterle, and Salomon, editors. *Ultracold Fermi Gas*. IOS Press, Amsterdam, 2007.

[26] J.F. James. *A Student's Guide to Fourier Transform*. Cambridge, New York, 2011.

[27] W. Koch and M.C. van der Holthausen. *A Chemist's Guide to Density Functional Theory*. Wiley-VHC Verlag, Germany, 2001.

[28] W. Kohn and L.J. Sham. Self-consistent equations including exchange and correlation effects. *Physical Review*, 140(4A), 1965.

[29] E.H. Lieb. Variational principle for many-fermion systems. *Phys. Rev. Lett.*, 46(7), 1981.

[30] F. London. The λ-phenomenon of liquid helium and the Bose-Einstein degeneracy. *Nature*, 141:643–644, 1938.

[31] G.D. Mahan. *Applied Mathematics*. Springer Science+Business Media, New York, 2001.

[32] H.J. Metcalf and P. van der Straten. *Laser Cooling and Trapping*. Springer-Verlag, New York, 1999.

[33] G.P. Parr and W. van der Yang. *Density-Functional Theory of Atoms and Molecules*. Oxford, New York, 1989.

[34] C.J. Pethick and H. Smith. *Bose-Einstein Condensation in Dilute Gases*. Cambridge University Press, New York, 2008.

[35] L.P. Pitaevskii. Vortex lines in an imperfect Bose gas. *Journal of Experimental and Theoretical Physics*, 13:451–455, 1961.

[36] E.L. Raab, M. Prentiss, A. Cable, S. Chu, and D.E. Pritchard. Trapping of neutral sodium atoms with radiation pressure. *Physical Review Letter*, 59(23), 1987.

[37] L. Salasnich. Fermionic condensation in ultracold atoms, nuclear matter and neutron stars. http://arxiv.org/pdf/1308.0922v1.pdf. Accessed: 2013-11-24.

[38] R. Stowasser and R. Hoffmann. What do the Kohn-Sham orbitals and eigenvalues mean? *J. Am. Chem. Soc.*, 121:3414–3420, 1999.

[39] K. Stuhler, A. Griesmaier, T. Koch, M. Fattori, T. Pfau, S. Giovannazi, P. Pedri, and L. Santos. Observation of dipole-dipole interaction in a degenerate quantum gas. *Phys. Rev. Lett.*, 95, 2005.

[40] L.H. Thomas. The calculation of atomic fields. *Mathematical Proceedings of the Cambridge Philosophical Society*, 23:542–548, 1927.

[41] A.G. Truscott, K.E. Strecker, W.I. McAlexander, G.B. Partridge, and R.G. Hulet. Observation of Fermi pressure in a gas of trapped atoms. *Science*, 291:2570–2572, 2001.

[42] M. Weidemüller and C. Zimmermann, editors. *Interactions in Ultracold Atoms*. Wiley - VCH Verlag, Weinheim, 2003.

[43] C. Zhao, L. Jiang, X. Liu, W.M. Liu, X. Zou, and H. Pu. Hartree-Fock-Bogoliubov theory of dipolar Fermi gases. *Phys. Rev. A.*, 81(6), 2010.